

A new, zero-iteration analytic implementation of wet-bulb globe temperature: development, validation and comparison with other methods

Qinqin Kong¹ and Matthew Huber¹

¹Purdue University

March 15, 2024

Abstract

Wet-bulb globe temperature (WBGT)—a standard measure for workplace heat stress regulation—incorporates the complex, nonlinear interaction among temperature, humidity, wind and radiation. This complexity requires WBGT to be calculated iteratively following the recommended approach developed by Liljegren and colleagues. The need for iteration has limited the wide application of Liljegren’s approach, and stimulated various simplified WBGT approximations that do not require iteration but are potentially seriously biased. By carefully examining the self-nonlinearities in Liljegren’s model, we develop a zero-iteration analytic approximation of WBGT while maintaining sufficient accuracy and the physical basis of the original model. The new approximation slightly deviates from Liljegren’s full model—by less than 1oC in 99\% cases over 93\% of global land area. The annual mean and 75-99\% percentiles of WBGT are also well represented with biases within ± 0.5 oC globally. This approximation is clearly more accurate than other commonly used WBGT approximations. Physical intuition can be developed on the processes controlling WBGT variations from an energy balance perspective. This may provide a basis for applying WBGT to understanding the physical control of heat stress.

Abstract

Wet-bulb globe temperature (WBGT)—a standard measure for workplace heat stress regulation—incorporates the complex, nonlinear interaction among temperature, humidity, wind and radiation. This complexity requires WBGT to be calculated iteratively following the recommended approach developed by Liljegren and colleagues. The need for iteration has limited the wide application of Liljegren’s approach, and stimulated various simplified WBGT approximations that do not require iteration but are potentially seriously biased. By carefully examining the self-nonlinearities in Liljegren’s model, we develop a zero-iteration analytic approximation of WBGT while maintaining sufficient accuracy and the physical basis of the original model. The new approximation slightly deviates from Liljegren’s full model—by less than 1°C in 99% cases over 93% of global land area. The annual mean and 75-99% percentiles of WBGT are also well represented with biases within $\pm 0.5^\circ\text{C}$ globally. This approximation is clearly more accurate than other commonly used WBGT approximations. Physical intuition can be developed on the processes controlling WBGT variations from an energy balance perspective. This may provide a basis for applying WBGT to understanding the physical control of heat stress.

Plain Language Summary

Wet-bulb globe temperature (WBGT) is a standard way to measure heat stress in the workplace. It incorporates the complex, nonlinear interactive effects of temperature, humidity, wind and radiation. This complexity requires WBGT to be calculated iteratively which is computationally intensive and less straightforward to implement algorithmically. To address these issues, we came up with a simplified version of WBGT that obviates the need for iteration. This simplified approach is computationally straightforward and also highly accurate.

1 Introduction

Heat stress presents significant threats to human health (Ebi et al., 2021; Buzan & Huber, 2020; Kjellstrom et al., 2016) with wide-ranging social (Hsiang et al., 2013; Burke et al., 2018) and economic consequences (Burke et al., 2015; Saeed et al., 2022). Metrics that accurately represent the physiological impact of heat stress are crucial for the monitoring, early warning, and impact assessment of heat stress (Havenith & Fiala, 2015; Simpson et al., 2023). Over the last century, numerous heat stress metrics have been formulated (de Freitas & Grigorieva, 2015), among which the wet-bulb globe temperature (WBGT) emerges as a notably comprehensive measure, encapsulating the interplay of temperature, humidity, wind speed and radiation effects (Yaglou & Minard, 1957). Rooted in physiology principles and fortified by empirical calibration, WBGT is as good or better than most other metrics in predicting human heat stress compensability (Vecellio et al., 2022), assessing the physiological influences of heat stress (Ioannou et al., 2022), and capturing the interactive effects of multiple meteorological factors on human physical work capacity (Foster et al., 2022, 2022). It has been incorporated into several heat stress regulatory standards across various domains including occupational health (NIOSH, 2016; ISO, 2017; OSHA, 2017), military operations (Army, 2003) and athletic activities (ACSM, 1984).

WBGT is defined as

$$WBGT = 0.7T_{nw} + 0.2T_g + 0.1T_a \quad (1)$$

under outdoor conditions where T_{nw} , T_g and T_a refer to natural wet-bulb temperature, black globe temperature and dry-bulb temperature respectively. The WBGT model developed by Liljegren et al. (2008) is the recommended approach for WBGT calculation due to its foundation on heat and mass transfer principles, careful treatment of the geometry of WBGT sensors, and extensive validation (RMSE $< 1^\circ\text{C}$) (Liljegren et al., 2008;

62 Lemke & Kjellstrom, 2012; Patel et al., 2013; Clark & Konrad, 2023). It derives T_{nw} and
 63 T_g by solving the nonlinear energy balance equations of the wet wick and black globe
 64 sensors. However, this process requires iterative calculations which have limited the widespread
 65 adoption of Liljegren’s approach. Even in recent work, a preference for simpler WBGT
 66 approximations that avoid iteration persists within the scientific community (e.g., Zhu
 67 et al. (2021); Brimicombe et al. (2023); Tuholske et al. (2021); Orlov et al. (2023); Kamal
 68 et al. (2024)). However, these simplified approximations are so diverse in formulation that
 69 they generate substantially different estimates making the results from different stud-
 70 ies challenging to meaningfully compare (Lemke & Kjellstrom, 2012; Kong & Huber, 2022).
 71 Some approximations are based on statistical relationship rather than physics (Moran
 72 et al., 2001; Australian Bureau of Meteorology, 2010; Kamal et al., 2024). The Australian
 73 Bureau of Meteorology WBGT formulation (hereafter referred as *sWBGT*) (Australian
 74 Bureau of Meteorology, 2010) has been demonstrated to be systematically biased, but
 75 remain widely used because of their simplicity (Kong & Huber, 2022). The generated
 76 heat stress estimates have been fed into impact models for assessing downstream social-
 77 economic consequences (Zhang & Shindell, 2021; Chavaillaz et al., 2019; Zhu et al., 2021;
 78 Matsumoto et al., 2021; de Lima et al., 2021). The propagation of biases stemming from
 79 these WBGT approximations through the chain of climate change impact assessment could
 80 potentially mislead policy-making pertaining to heat stress mitigation and adaptation.

81 We aim to address this issue by developing a simplified WBGT model that does
 82 not require iteration while maintaining sufficient accuracy and physics of heat and mass
 83 transfer. This is achieved with an analytic approximation of Liljegren’s WBGT through
 84 substituting reasonable first-guess values of T_{nw} and T_g into the energy balance equa-
 85 tions of the wet wick and black globe sensors. The analytic approximation will be eval-
 86 uated against Liljegren’s full model which, although subject to biases compared to field
 87 observations (Lemke & Kjellstrom, 2012; Patel et al., 2013; Liljegren et al., 2008; Clark
 88 & Konrad, 2023), is treated as ground truth in this paper.

89 The remainder of this paper is structured as follows. Section 2 provides a concise
 90 overview of Liljegren’s WBGT model focusing on the nonlinear energy balance equations.
 91 Section 3 introduces the analytic approximation of WBGT the accuracy of which is eval-
 92 uated in Section 4. This evaluation is first conducted with synthetic data to understand
 93 the bias structure across the multidimensional parameter space encompassing temper-
 94 ature, humidity, solar radiation and wind speed (Section 4.1). We then explore the mag-
 95 nitude and spatial distribution of biases within a more realistic context (Section 4.2). This
 96 is primarily done with ERA5 reanalysis (Hersbach, H. et al., 2018) for a historical pe-
 97 riod, supplemented by the ACCESS-CM2 model (Dix et al., 2019) for a warmer climate.
 98 Afterwards, we compare this analytic approximation against other commonly used ap-
 99 proximations of WBGT (Section 4.3). Section 5 contains a brief summary and implica-
 100 tions on applying WBGT to understanding physical processes controlling heat stress.

101 2 Liljegren WBGT model

102 Here we briefly review the T_g and T_{nw} formulations in Liljegren’s WBGT model
 103 while directing interested readers to Liljegren et al. (2008) and Kong and Huber (2022)
 104 for details.

105 2.1 Black globe temperature

106 The energy balance equation for the black globe is given by

$$\sigma\epsilon_g T_g^4 + h_{cg}(T_g - T_a) = LR_g + SR_g \quad (2)$$

107 where energy gain from incoming thermal (LR_g) and solar radiation (SR_g) is balanced
 108 by long-wave cooling and energy loss through convective heat transfer between the globe
 109 and ambient air corresponding respectively to the two terms on the left side of Eq. 2.

110 Note that LR_g encompasses both downward and upwelling thermal radiation; SR_g also
 111 integrates heating from both downward (direct and diffuse) and ground surface reflected
 112 solar radiation, and incorporates parameters representing solar zenith angle, albedo of
 113 the globe and ground surface, and globe geometry characteristics. Please refer to Liljegren
 114 et al. (2008) and Kong and Huber (2022) for the formulations of LR_g and SR_g . h_{cg} sig-
 115 nifies convective heat transfer coefficient associated with the globe; σ and ϵ_g stand for
 116 the Stefan-Boltzmann constant and emissivity of the globe. Eq. 2 is analogous to to Eq.
 117 15 in Liljegren et al. (2008), although the long-wave and surface reflected short-wave ra-
 118 diation embedded within LR_g and SR_g will be obtained directly from climate model out-
 119 put as was done in Kong and Huber (2022). In Liljegren's original approach, these ra-
 120 diative fluxes are approximated from temperature, humidity and ground surface albedo.

121 Eq. 2 can be rearranged into

$$T_g = T_a + \frac{SR_g + LR_g - \sigma\epsilon_g T_a^4}{h_{cg} + h_{rg}} \quad (3)$$

122 where h_{rg} can be interpreted as a thermal radiative heat transfer coefficient

$$h_{rg} = \sigma\epsilon_g(T_g^2 + T_a^2)(T_g + T_a)$$

123 Note that $LR_g - \sigma\epsilon_g T_a^4$ is typically small and actually approaches zero when the
 124 downward and upward thermal radiation can be represented by a mean radiant temper-
 125 ature of T_a in absence of solar radiation. With this term being neglected, we have

$$T_g - T_a = \frac{SR_g}{h_{cg} + h_{rg}} \quad (4)$$

126 The physical interpretation of Eq. 4 is that the efficiency of energy loss through
 127 long-wave cooling (h_{rg}) and convection (h_{cg}) modulates the required temperature gra-
 128 dient between the globe and ambient air in order to balance the energy gain from solar
 129 radiation.

130 Eq. 3 cannot be solved analytically since both h_{cg} and h_{rg} depend nonlinearly on
 131 T_g (i.e., Eq. 3 is self-nonlinear in T_g). h_{cg} is derived from the empirical correlation for
 132 heat transfer from a sphere in cross flow (Brenda Jacklitsch et al., 2016) (see Eq. 16 in
 133 Liljegren et al. (2008) for its formulation). It is mainly affected by wind speed but also
 134 depends on film temperature (T_f) which is the temperature of the air within the con-
 135 vective boundary layer proximate to the surface of the globe, and is calculated as the
 136 arithmetic mean between the temperatures of the globe surface and ambient air ($T_f =$
 137 $(T_g + T_a)/2$). Consequently, Eq. 3 needs to be solved by iteration to obtain the equi-
 138 librium T_g . In Section 3.1, we will provide an analytic solution to T_g which does not re-
 139 quire iteration.

140 2.2 Natural wet-bulb temperature

141 The energy balance equation for the wick is

$$k_x \frac{e_w - e_a}{P - e_w} M_{H_2O} \Delta H + h_{cw}(T_{nw} - T_a) + \sigma\epsilon_w T_{nw}^4 = LR_w + SR_w \quad (5)$$

142 where the radiative energy gain on the right side of the equation is balanced by en-
 143 ergy loss through evaporating water, convection, and thermal radiation corresponding
 144 respectively to the three terms on the left side of the equation. The convective heat trans-
 145 fer coefficient h_{cw} is obtained from the empirical correlation for heat transfer from a cylin-
 146 der (Bedingfield & Drew, 1950). k_x denotes convective mass transfer coefficient which
 147 are interconnected with h_{cw} via the Chilton-Colburn analogy (Chilton & Colburn, 1934).

148 They are both predominantly affected by wind speed with weak dependence on film tem-
 149 perature ($T_f = (T_a + T_{nw})/2$) (see Eq. 8 and 10 in Liljegren et al. (2008) for their for-
 150 mulations). e_a and e_w represent ambient vapor pressure and the saturation vapor pres-
 151 sure at the temperature of the wick ($e_w = e_{sat}(T_{nw})$); P is surface pressure; M_{H_2O} is
 152 the molecular weight of water vapor; ΔH stands for the heat of vaporization.

153 Eq. 5 can be rearranged into

$$T_{nw} = T_a + \frac{SR_w - \beta(e_{sat}(T_a) - e_a) + LR_w - \sigma\epsilon_w T_a^4}{h_{ew} + h_{cw} + h_{rw}} \quad (6)$$

154 where β is defined as

$$\beta = \frac{k_x M_{H_2O} \Delta H}{P - e_w} \approx \frac{k_x M_{H_2O} \Delta H}{P}$$

155 h_{ew} and h_{rw} can be interpreted as evaporative and thermal radiative heat trans-
 156 fer coefficients for the wick cylinder, and are defined as

$$h_{ew} = \beta \frac{e_w - e_{sat}(T_a)}{T_{nw} - T_a} \approx \beta \left. \frac{\partial e_{sat}(T)}{\partial T} \right|_{T = \frac{T_{nw} + T_a}{2}} \quad (7)$$

157

$$h_{rw} = \sigma\epsilon_w (T_{nw}^2 + T_a^2)(T_{nw} + T_a)$$

158 Note that h_{ew} , by definition, measures the efficiency of evaporative heat transfer
 159 between the wet wick and a saturated air. The fact that air can be under-saturated cre-
 160 ates a cooling term from vapor pressure deficit (VPD) ($\beta(e_{sat}(T_a) - e_a)$ in Eq. 6).

161 With $LR_w - \sigma\epsilon_w T_a^4$ being typically small and neglected, we have

$$T_{nw} - T_a = \frac{SR_w - \beta(e_{sat}(T_a) - e_a)}{h_{ew} + h_{cw} + h_{rw}} \quad (8)$$

162 Namely, the temperature gradient between the wick and ambient air is driven by net en-
 163 ergy input from solar radiation and VPD, regulated by the efficiency of energy loss via
 164 evaporation (h_{ew}), convection (h_{cw}) and long-wave cooling (h_{rw}).

165 Similar to the case of T_g , Eq. 6 needs to be solved by iteration because both the
 166 mass transfer (k_x) and three heat transfer coefficients (h_{ew} , h_{cw} and h_{rw}) depend non-
 167 linearly on T_{nw} . An analytic approximation to T_{nw} will be provided in Section 3.2 by
 168 removing the self-nonlinearity.

169 3 Analytic approximation of wet-bulb globe temperature

170 In the previous section, we established that both T_g and T_{nw} cannot be solved an-
 171alytically because they are embedded nonlinearly within the mass and heat transfer co-
 172efficients. Numerical solutions can be pursued through iterative methods: starting with
 173an initial guess, inserting it into the transfer coefficients within Eq. 3 or 6, obtaining an
 174updated value, and iteratively repeating this process until consecutive updates deviate
 175by less than a specified tolerance. However, we argue that employing a judicious initial
 176guess might yield a result that is sufficiently accurate, thereby eliminating the need for
 177iterations. By employing this approach, Eq. 3 and 6 become analytic formulations of T_g
 178and T_{nw} , and the ensuing solutions are henceforth referred to as analytic approximations.

179 3.1 Black globe temperature

180 An analytic approximation of T_g can be obtained by substituting a certain first-
 181guess value of T_g into h_{cg} and h_{rg} on the right side of Eq. 3. Ideally, the first-guess value
 182should be close to T_g , but this is less critical due to reasons articulated below.

183 h_{cg} is derived from empirical correlations under forced convection with surround-
 184 ing fluid motion (Liljegren et al., 2008), and therefore is primarily dictated by wind speed
 185 with minimal sensitivity to film temperature (Fig. 1a and d). This choice is justified by
 186 the dominance of forced convection over free convection under non-negligible wind speeds
 187 and reasonable temperature gradients between the globe and ambient air (Gao et al.,
 188 2019). Under a wind speed of 2 m/s, a 10 °C increase of film temperature from 30 to 40
 189 °C only cause a 0.2% reduction in h_{cg} (Fig. 1d). In fact, the international standard ISO
 190 7726 (ISO, 1998) parameterizes convective heat transfer coefficients under forced con-
 191 vection as solely a function of wind speed. On the other hand, h_{rg} only varies by around
 192 0.5% per °C change in T_g , and energy loss via thermal radiation is typically 2-5 times
 193 less efficient than convection (Fig. 1a).

194 The minor influence of temperature on h_{cg} and small fractional changes in h_{rg} with
 195 temperature suggest that the initial estimate's proximity to the true value is not crit-
 196 ical. Therefore, we choose T_a as a first guess for T_g for simplicity. The resultant approx-
 197 imations to both heat transfer coefficients are denoted as \widehat{h}_{cg} and \widehat{h}_{rg} the latter of which
 198 is calculated as $\widehat{h}_{rg} = 4\sigma\epsilon_g T_a^3$. For \widehat{h}_{cg} , film temperature is approximated by $T_f = \frac{T_g + T_a}{2} \approx$
 199 T_a . Consequently, we have an analytic approximation of T_g :

$$\widehat{T}_g = T_a + \frac{SR_g + LR_g - \sigma\epsilon_g T_a^4}{\widehat{h}_{cg} + \widehat{h}_{rg}} \quad (9)$$

200 The accuracy of \widehat{T}_g can be assessed by comparing it against the true value of T_g in Eq.
 201 3.

$$\widehat{T}_g - T_g = (T_g - T_a) \frac{h_{cg} - \widehat{h}_{cg} + h_{rg} - \widehat{h}_{rg}}{\widehat{h}_{cg} + \widehat{h}_{rg}}$$

202 As explained above, the deviation of \widehat{h}_{cg} from h_{cg} is negligible, which simplifies the
 203 bias of \widehat{T}_g into

$$\begin{aligned} \widehat{T}_g - T_g &= (T_g - T_a) \frac{h_{rg} - \widehat{h}_{rg}}{\widehat{h}_{cg} + \widehat{h}_{rg}} \\ &= \frac{\sigma\epsilon_g (T_g - T_a)^2 [(T_g + T_a)^2 + 2T_a^2]}{\widehat{h}_{cg} + \widehat{h}_{rg}} \end{aligned} \quad (10)$$

204 It is clear that \widehat{T}_g always has non-negative biases the magnitude of which is proportional
 205 to the square of the temperature gradient between the globe and ambient air. There-
 206 fore, \widehat{T}_g is expected to perform better under conditions of weak solar radiation and high
 207 wind speed wherein the weaker solar heating and efficient convective heat transfer make
 208 T_g closer to T_a . Given T_g and T_a of $\sim 300\text{K}$ and $T_g - T_a$ of $\sim 20\text{K}$, the largest possible
 209 bias is $\sim 2\text{K}$ which can only be realized when $h_{cg} = 0$. However, the actual bias will be
 210 significantly smaller since h_{cg} is usually considerably larger than h_{rg} (Fig. 1a). The phys-
 211 ical interpretation of this formulation is that the approximation to long-wave cooling in-
 212 troduces minimal biases when convection is the dominant pathway for energy loss.

213 3.2 Natural wet-bulb temperature

214 An analytic solution for T_{nw} can be obtained by substituting a first-guess value of
 215 T_{nw} into the mass and three heat transfer coefficients in Eq. 6. Similar to the case of
 216 T_g , both k_x and h_{cw} exhibit minimal sensitivity to temperature variations (Fig. 1b-d).
 217 h_{rw} only varies by 0.5% per °C change in T_{nw} and energy loss via thermal radiation is
 218 much less efficient than convection and evaporation (Fig. 1b). Therefore, the proxim-
 219 ity of the first guess to the true T_{nw} is less critical for mass transfer and heat transfer

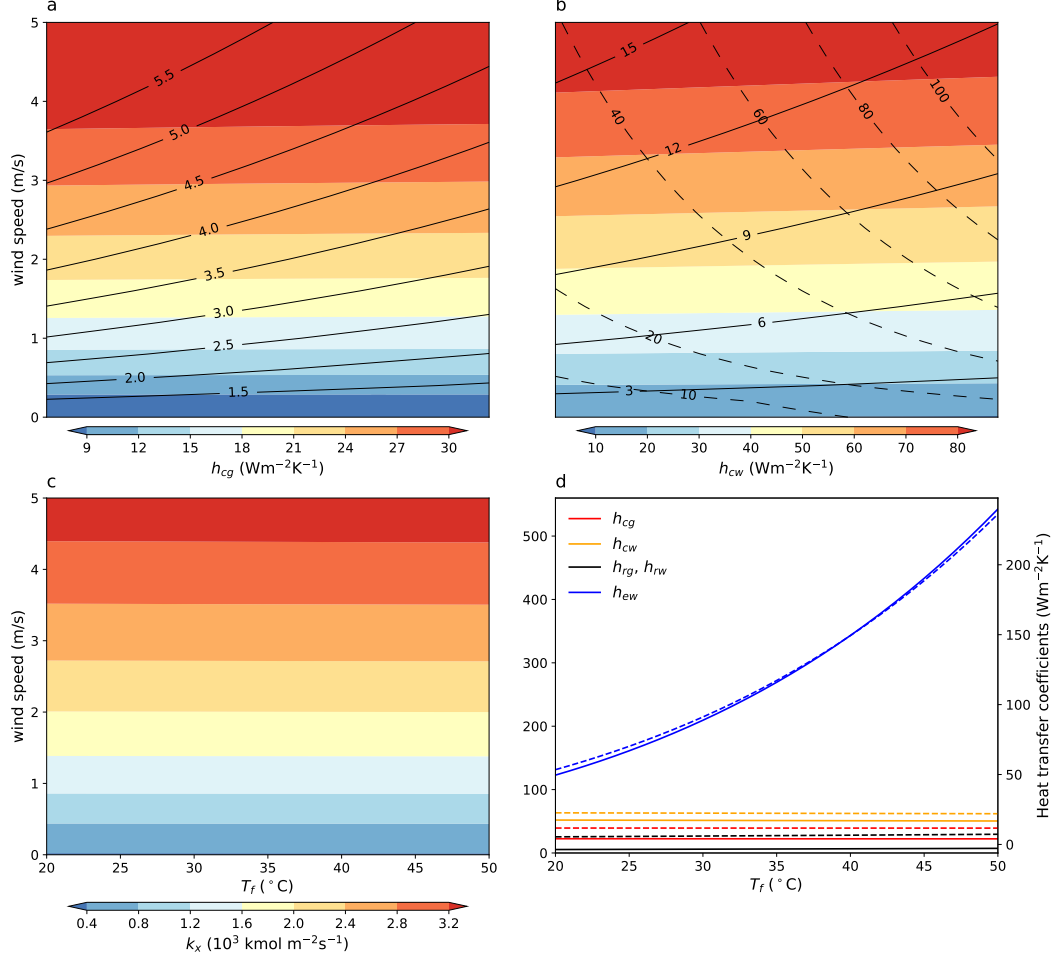


Figure 1. Shadings in (a)-(c) denote h_{cg} , h_{cw} and k_x respectively. Solid contours in (a) and (b) represent the ratio between convective and thermal radiative heat transfer coefficients for the black globe (h_{cg}/h_{rg}) and wick cylinder (h_{cw}/h_{rw}). Dashed contours in (b) represent the ratio between h_{ew} and h_{rw} . Values in panel (a)-(c) are expressed as functions of film temperature and wind speed. (d) Various heat transfer coefficients for the globe and wick as functions of film temperature under a 2m/s (solid lines corresponding to left y-axis) and 0.5m/s (dashed lines corresponding to right y-axis) wind speed. Thermal radiative heat transfer coefficients are approximated as $h_{rg} \approx 4\sigma\epsilon_g T_f^3$ for the black globe and $h_{rw} \approx 4\sigma\epsilon_w T_f^3$ for the wet wick, with $\epsilon_g = \epsilon_w = 0.95$. Surface pressure has a minor impact on all heat transfer coefficients within its typical range of variation, and is fixed at 1000 hPa.

220 via convection and thermal radiation. However, it might be of greater concern for the
 221 evaporative heat transfer coefficient (Eq. 7), as h_{ew} varies by around 2-3% per °C change
 222 in T_{nw} , and evaporation is the most efficient energy loss pathway for the wet wick (Fig.
 223 1b and d).

224 Therefore, a reasonably good first guess for T_{nw} is needed. We choose the wet-bulb
 225 temperature (T_w) which is very close to T_{nw} at night and typically remains within 3°C
 226 below T_{nw} during the day, depending on solar radiation intensity (Fig. 5b). For the sake
 227 of computational efficiency and analytic tractability, we calculate T_w from temperature
 228 and relative humidity using an empirical formula developed by Stull (2011). Stull's T_w
 229 is subject to around 1°C overestimation at high temperatures, commonly occurring dur-
 230 ing the day (Buzan et al., 2015). This slight overestimation actually brings Stull's T_w
 231 closer to T_{nw} and provides a better initial guess. The resulting analytic approximation
 232 is

$$\widehat{T}_{nw} = T_a + \frac{SR_w - \widehat{\beta}(e_{sat}(T_a) - e_a) + LR_w - \sigma\epsilon_w T_a^4}{\widehat{h}_{ew} + \widehat{h}_{cw} + \widehat{h}_{rw}} \quad (11)$$

233 where $\widehat{\beta} = \widehat{k}_x M_{H_2O} \Delta H / P$. By comparing against Eq. 6, we quantify the bias of
 234 \widehat{T}_{nw}

$$\widehat{T}_{nw} - T_{nw} = \eta(T_{nw} - T_a)(T_{nw} - T_w) \quad (12)$$

235

$$\eta = \frac{\frac{1}{2}\beta \frac{\partial^2 e_{sat}(T)}{\partial T^2} \Big|_{T=\frac{T_{nw}+T_w+2T_a}{4}} + \sigma\epsilon_w(T_{nw}^2 + T_w^2 + T_a^2 + T_{nw}T_w + T_aT_{nw} + T_aT_w)}{\widehat{h}_{ew} + \widehat{h}_{cw} + \widehat{h}_{rw}}$$

236 where we assume $\widehat{k}_x \approx k_x$ and $\widehat{h}_{cw} \approx h_{cw}$ since both the convective mass and
 237 heat transfer coefficients are extremely insensitive to variations in film temperature (Fig.
 238 1b-d). Since $T_{nw} \geq T_w$, \widehat{T}_{nw} is subject to overestimation when $T_{nw} > T_a$ and under-
 239 estimation otherwise. By inspection, it is clear that the magnitude of biases increases
 240 with enlarging differences between T_{nw} and both T_a and T_w . Over subtropical hot-dry
 241 regions, the strong VPD cooling and solar radiative heating are expected to enlarge both
 242 temperature gradients with $T_{nw} < T_a$ and $T_{nw} > T_w$ leading to relatively strong neg-
 243 ative biases in \widehat{T}_{nw} .

244 3.3 Wet-bulb globe temperature

245 Substituting \widehat{T}_g (Eq. 9) and \widehat{T}_{nw} (Eq. 11) back into Eq. 1, we obtain the analytic
 246 approximation to WBGT

$$WBGT = 0.7\widehat{T}_{nw} + 0.2\widehat{T}_g + 0.1T_a \quad (13)$$

247 \widehat{T}_g , \widehat{T}_{nw} and $WBGT$ are referred as analytic approximations in the sense that self-
 248 nonlinearities in T_g and T_{nw} within the energy balance equations are eliminated by sub-
 249 stituting initial estimates of them into the mass and/or heat transfer coefficients. This
 250 permits WBGT to be expressed as an analytic function of temperature, humidity, wind
 251 and radiation, although this function remains highly complex and nonlinear.

252 4 Validation of the analytic approximation

253 The validation of the analytic approximation is undertaken in both an idealized
 254 and a more realistic context by comparing against results from Liljegren's full model driven

255 by atmospheric variable inputs. In the idealized setting, we investigate the bias struc-
 256 ture of the analytic approximation across a multidimensional parameter space of air tem-
 257 perature, wind speed, relative humidity and incoming solar radiation based on synthetic
 258 data. We highlight the environmental conditions that yield relatively large biases.

259 Next, we examine the magnitude and spatial distribution of biases within a more
 260 realistic setting using ERA5 reanalysis (Hersbach, H. et al., 2018) for the period 2013-
 261 2022 as the inputs. Since we aim to use this approximate framework in a range of cli-
 262 mate states, including a much warmer future, we also validate it against a "hot" CMIP6
 263 simulation. This is conducted for the period 2091-2100 under the SSP585 scenario us-
 264 ing the ACCESS-CM2 model (Dix et al., 2019) which has a relatively high equilibrium
 265 climate sensitivity of 4.7°C (Hausfather, 2019). The data is evaluated at hourly inter-
 266 vals for ERA5 and 3-hourly for ACCESS-CM2 at their original grid spacing. WBGT is
 267 calculated from 2m air temperature and humidity, 10m wind speed, surface pressure, as
 268 well as surface downward and upwelling flux of long-wave and short-wave radiation.

269 4.1 Validation and bias characterization: idealized setting

270 The accuracy of the analytic approximation is evaluated across a range of air tem-
 271 perature (20-50°C) and wind speed (0.13-3 m/s) under different levels of relative humid-
 272 ity (20% and 60%) and incoming solar radiation (0, 450, and 900 W/m²) (Fig. 2).

273 \widehat{T}_g slightly overestimates T_g in Liljegren's full model by less than 0.2 °C during night-
 274 time and under conditions of moderate solar radiation (450W/m²). However, as solar
 275 radiation intensifies and wind speed diminishes, the degree of overestimation becomes
 276 more pronounced. It can exceed 1 °C under scenarios of strong solar radiation (900 W/m²)
 277 and low wind speed (< 0.5m/s) (Fig. 2a). This intensification of overestimation can be
 278 attributed to the increased temperature gradient between the black globe and the amb-
 279 ient air (as illustrated in Eq. 10) due to intense solar heating and less effective energy
 280 loss through convection under low wind speed. In practice, the relatively large overes-
 281 timation under low wind speed is less a concern as the movement of human body cre-
 282 ates relative air flow especially for outdoor workers. In fact, prior studies frequently as-
 283 sume a minimum wind speed of 1m/s when assessing heat stress-induced labor loss (Casanueva
 284 et al., 2020; Kjellstrom et al., 2018; Bröde et al., 2018).

285 \widehat{T}_{nw} has small biases (within $\pm 0.2^\circ\text{C}$ of T_{nw} in Liljeren's full model) at nighttime
 286 when T_w , our initial estimate, is close to T_{nw} (Fig. 5b). At daytime, \widehat{T}_{nw} performs well
 287 under wet condition (60% relative humidity). However, under dry condition (20% rel-
 288 ative humidity), \widehat{T}_{nw} shows substantial underestimations especially under lower wind speed
 289 and higher temperature where the underestimation can extend up to -2°C. This can be
 290 attributed to a strong temperature gradient between the wet wick and the ambient air
 291 ($T_{nw} - T_a$) under hot-dry conditions with low wind speed (as illustrated in Eq. 12). The
 292 underestimation also intensifies under stronger solar radiation probably owing to an en-
 293 larged difference between T_{nw} and T_w .

294 Biases in \widehat{WBGT} are expected to be primarily influenced by biases in \widehat{T}_{nw} , given
 295 that T_{nw} contributes 70% to WBGT. Accordingly, we found that \widehat{WBGT} shares a simi-
 296 lar bias structure with \widehat{T}_{nw} , but the magnitudes are smaller and within $\pm 0.8^\circ\text{C}$ across
 297 the selected ranges of meteorological conditions (Fig. 2c).

298 4.2 Validation and bias characterization: realistic setting

299 The bias characterization within the idealized setting demonstrates the structure
 300 of biases in the analytic approximations across a range of meteorological conditions. In
 301 practice, those meteorological conditions are not equally sampled with some combina-
 302 tions of temperature, humidity, solar radiation and/or wind speed more or less likely. It

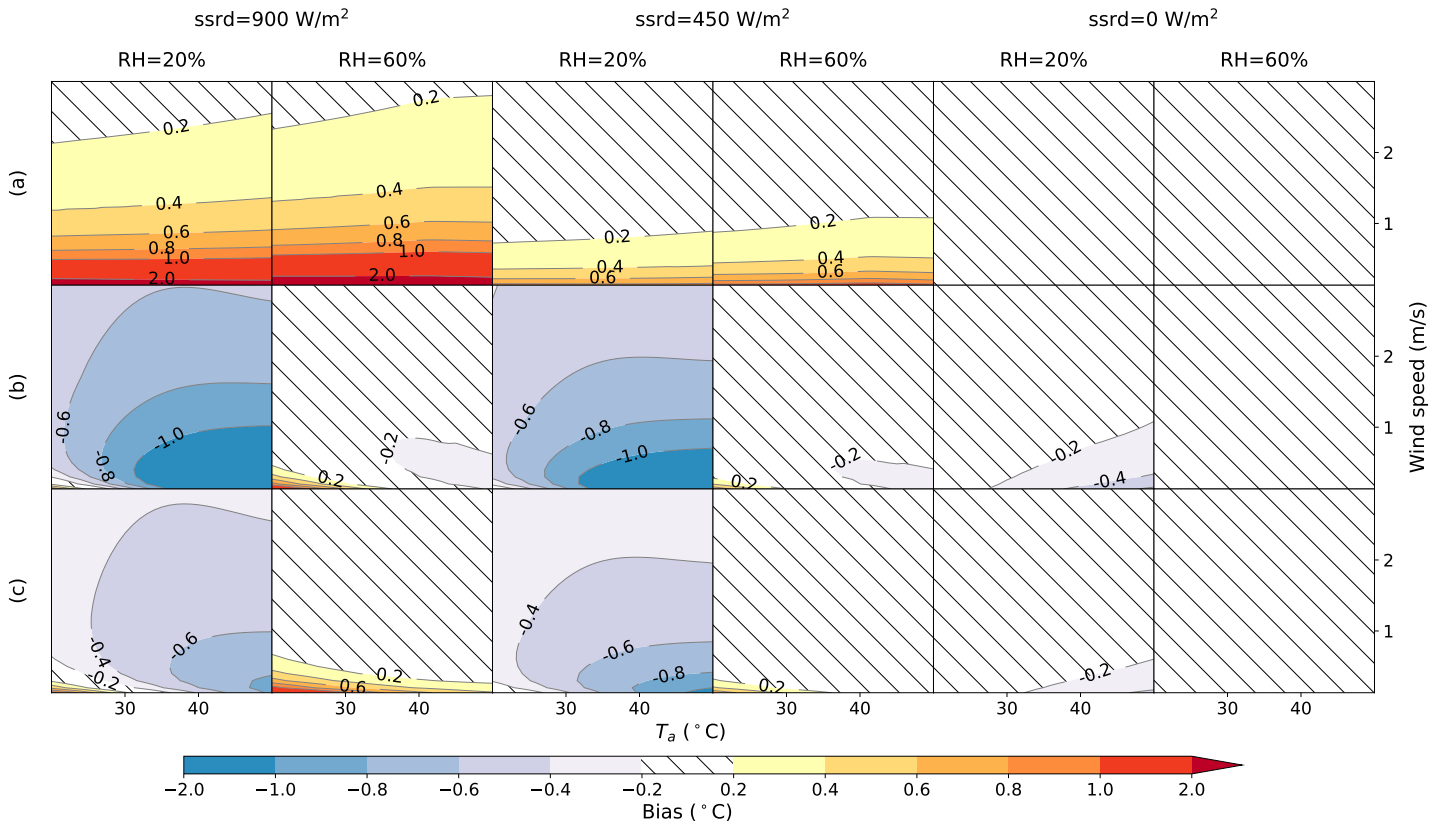


Figure 2. Biases in analytic approximations of (a) T_g , (b) T_{nw} and (c) WBGT across the parameter space covering selected ranges of temperature (T_a) (20-50°C), wind speed (0.13-3m/s), relative humidity (RH) (20%, 60%) and incoming solar radiation (ssrd) (0, 450, 900W/m²). Biases are evaluated against Liljegren’s full model. Thermal radiation and surface reflected solar radiation are approximated from temperature, relative humidity and an assumed surface albedo following the original formulation of Liljegren et al. (2008).

303 is of interest to examine the likely magnitudes and spatial distribution of biases in more
 304 realistic settings.

305 Figure 3 shows the area-weighted empirical distribution of biases in \widehat{WBGT} over
 306 land. During the period 2013-2022 of ERA5, around 78% of the total samples have bi-
 307 ases within $\pm 0.1^\circ\text{C}$, while this percentage extends to 97% for biases within $\pm 0.5^\circ\text{C}$. A
 308 similar level of accuracy is maintained in a warmer world with 93% of samples falling
 309 within $\pm 0.5^\circ\text{C}$. Although the peak of the distribution around zero becomes lower, accom-
 310 panied by a slightly fatter tail on the side of negative biases (Fig. 3), it is unclear whether
 311 this accuracy reduction can be attributed to climate change (Sherwood & Huber, 2010;
 312 Williams et al., 2009), or due to potential effects from other confounding factors such
 313 as the distinct spatial resolutions between ERA5 and ACCESS-CM2. For our purpose
 314 however, the method is sufficiently accurate across a wide range of climates.

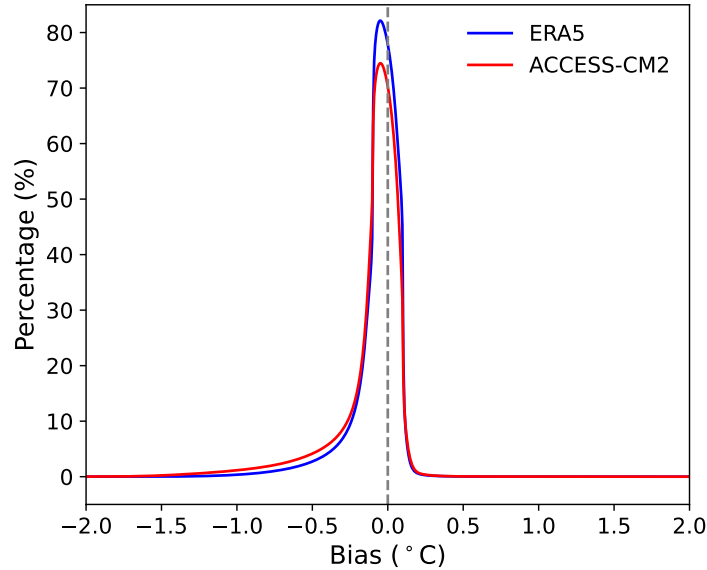


Figure 3. Empirical probability distribution of biases in our analytic approximation \widehat{WBGT} . The y-axes are designed to represent the percentage of samples showing biases within a 0.2°C interval centered on the corresponding x coordinates. The empirical distribution is derived from land data weighted by grid-cell area using ERA5 reanalysis for the period 2013-2022 and the ACCESS-CM2 model for the period 2091-2100 under the SSP585 scenario. Samples with \widehat{WBGT} below 15°C are excluded, as they are less relevant to heat stress.

315 Using ERA5, we then highlight the annual 1% and 99% percentile of these biases,
 316 thereby directing attention to the tails of the bias distribution and their spatial patterns
 317 (Fig. 4). \widehat{T}_g , as demonstrated in Eq. 10, is only subject to overestimations the 1% per-
 318 centile of which is close to zero (Fig. 4a). The 99% percentile of the overestimations is
 319 within 1°C over 97% of global land area (Fig. 4b and k). Over some alpine areas, like
 320 the Himalayas, strong solar radiation stemming from an optically thin atmosphere leads
 321 to large disparities between T_g and T_a , thereby causing relatively strong overestimations
 322 ($>1.8^\circ\text{C}$) (Fig. 4b).

323 In comparison, \widehat{T}_{nw} , can cause both under- and overestimations. The 1% percentile
 324 of biases is characterized by underestimations within -1°C over 85% of land area (Fig.
 325 4d and j). Over subtropical dry regions, strong VPD and solar radiation make T_{nw} sub-
 326 stantially smaller than T_a and larger than T_w which induces more pronounced under-

estimations by \widehat{T}_{nw} (Fig. 4d) as demonstrated in Eq. 12. The 99% percentile of biases show weak overestimations within 0.6°C over 92% of land area (Fig. 4e and k). Over the Himalayas alpine region, small VPD (as a result of cold temperature) and strong solar radiation make T_{nw} considerably larger than both T_a and T_w leading to relatively strong overestimations (Fig. 4e).

\widehat{WBGT} shares a similar spatial distribution of biases as \widehat{T}_{nw} with the 1% percentile of biases showing underestimations within -1°C over 96% of land area (Fig. 4g and j), and the 99% percentile characterized by overestimations within 0.6°C over 94% of land area (Fig. 4h and k).

We also show the 99% percentile of the absolute values of biases in the analytic approximations (Fig. 4 c, f, i and l) in order to highlight the upper tail of the magnitudes of their deviations from Liljegren's full model. In 99% cases, biases in \widehat{T}_g , \widehat{T}_{nw} and \widehat{WBGT} are limited within $\pm 1^\circ\text{C}$ over 97%, 82% and 93% of land area. It is also of interest to know the performance of our analytic approximation in representing heat stress at the levels of annual mean and different percentiles. As shown in figure 6q-t, \widehat{WBGT} can well represent heat stress across annual mean and 75%, 90% and 99% percentiles with biases within $\pm 0.5^\circ\text{C}$ globally.

4.3 Comparison against other approximations

We compare \widehat{WBGT} against several other WBGT approximations commonly used in the literature. These include sWBGT which only contains temperature and humidity while assuming moderately strong solar radiation and low wind speeds (Australian Bureau of Meteorology, 2010), the environmental stress index (ESI), derived through a multivariate regression of WBGT against temperature, incoming solar radiation, and relative humidity (Moran et al., 2001), the indoor WBGT ($WBGT_{in}$) which substitutes T_{nw} with the thermodynamic wet-bulb temperature (T_w) and T_g with T_a (Dunne et al., 2013; C. Li et al., 2020; D. Li et al., 2020), and the one recently developed by Brimicombe et al. (2023) ($WBGT_{Br}$) which calculates T_g from mean radiant temperature, and approximates T_{nw} using Stull's T_w formulation (Stull, 2011).

Figure 5a illustrates the empirical bias distribution of these approximations along with that of our analytic approximation based on ERA5. \widehat{WBGT} clearly outperforms others. sWBGT performs the worst, and its bias distribution peaks at an overestimation of approximately 5°C due to the implicit assumption of moderately strong solar radiation. This overestimate can profoundly affect future heat stress projections and estimate of impact on people (de Lima et al., 2021). Therefore, we do not recommend the continued use of sWBGT. ESI performs significantly better with a relatively symmetric distribution of biases centered around zero.

The distribution of biases in both $WBGT_{in}$ and $WBGT_{Br}$ have a primary peak near zero as well as secondary peaks corresponding to underestimations of approximately -2.4°C and -1.2°C respectively (Fig. 5a). Both $WBGT_{in}$ and $WBGT_{Br}$ substitute T_{nw} with T_w , and $WBGT_{in}$ also approximates T_g with T_a . These approximations work relatively well during nighttime especially for T_{nw} (Fig. 5b). Notably, T_g is lower than T_a at nighttime, and the distribution of their differences peaks around -1°C , but can extend up to -3°C (Fig. 5b). That is because air is not a black body, and consequently the long-wave radiative exchange between the black globe and ambient air produce net cooling on the globe. However, during daytime, T_w and T_a significantly underestimate T_{nw} and T_g due to the omission of solar radiative heating. The distributions of these underestimations peak around -1.2°C and -7.6°C respectively (Fig. 5b) which amounts to underestimations in WBGT of -0.8°C and -1.5°C given the weights on T_{nw} and T_g in WBGT formulation. The differentiated daytime versus nighttime performances explain the bimodal distribution of biases in $WBGT_{in}$ and $WBGT_{Br}$ (Fig. 5a).

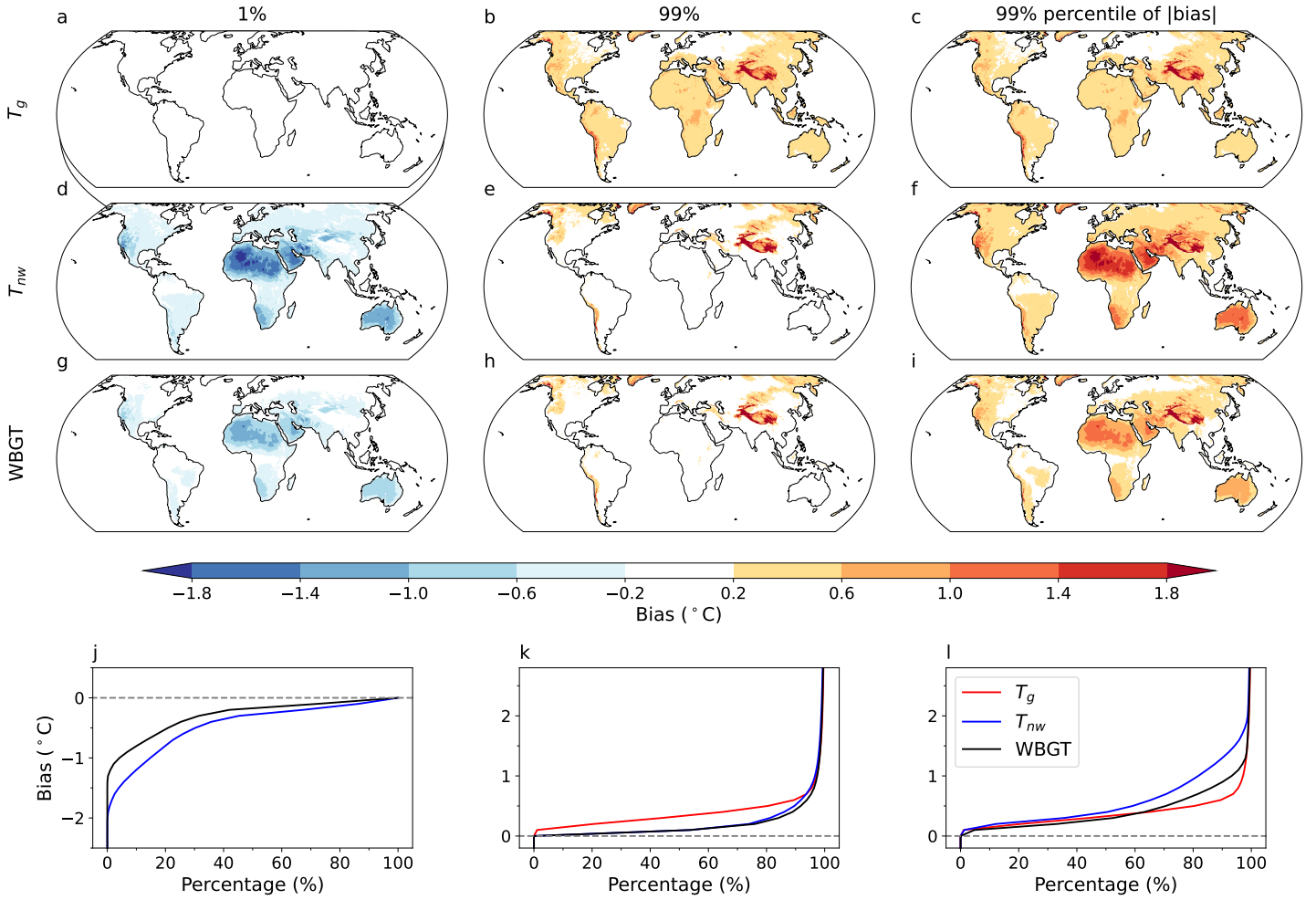


Figure 4. Annual (left) 1% and (middle) 99% percentile of biases, and (right) 99% percentile of the absolute magnitudes of biases in the analytic approximations of (a-c) T_g , (d-f) T_{nw} and (g-i) WBGT. Panels j-l represent the empirical cumulative distribution of these biases across all continental grid cells weighted by area. The 1% percentile of biases in \hat{T}_g are very close to zero and therefore are omitted in (j). Biases are evaluated by comparing against Liljegren’s full model based on hourly ERA5 reanalysis data during 2013-2022.

377 The shape of the bias distribution and the relative performance of different approx-
 378 imations remain consistent in a future warmer world, where \widehat{WBGT} continues to have
 379 the best performance (Fig. 5c).

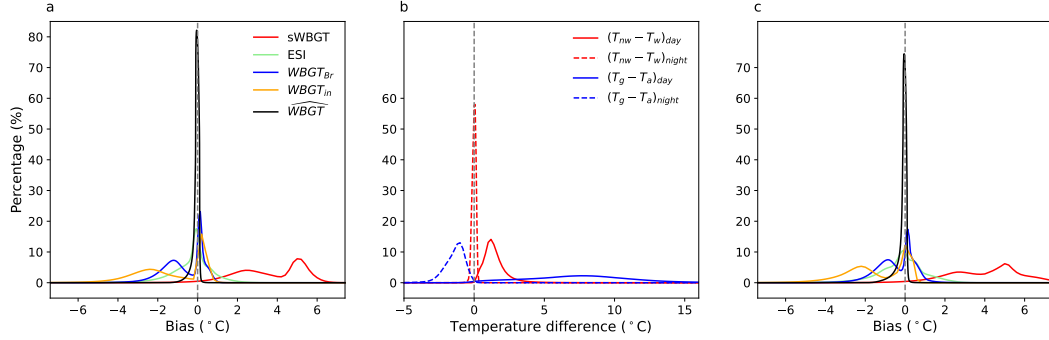


Figure 5. Empirical probability distribution of (a) biases in our analytic formulation \widehat{WBGT} and several other WBGT approximations, and (b) $T_{nw} - T_w$ and $T_g - T_a$ at both daytime and nighttime. Both (a) and (b) are derived from land data weighted by grid-cell area using ERA5 reanalysis for the period of 2013-2022. Panel (c) is the same as (a) except for the period 2091-2100 under the SSP585 scenario using the ACCESS-CM2 model. The y-axes are designed to represent the percentage of samples showing biases within a 0.2°C interval centered on the corresponding x coordinates. Samples with WBGT below 15°C are excluded, as they are less relevant to heat stress.

380 Our analytic approximation also performs better in representing the annual mean
 381 and 75-99% percentiles of WBGT with biases consistently within $\pm 0.5^\circ\text{C}$ across the world
 382 as described previously (Fig. 6). sWBGT strongly overestimates WBGT especially at
 383 annual mean level, and this overestimation becomes weaker towards higher percentiles
 384 where the assumption of moderately strong solar radiation becomes more applicable (Fig.
 385 6a-d). ESI performs well in capturing annual mean and 75% percentile of WBGT with
 386 biases mostly within $\pm 1^\circ\text{C}$, but considerably underestimates the 99% percentile by up
 387 to -4°C across the low latitudes (Fig. 6e-h). Both $WBGT_{in}$ and $WBGT_{Br}$ consistently
 388 show underestimations the magnitude of which increases towards higher percentiles (Fig.
 389 6i-p). Among them, $WBGT_{Br}$ has better performance since T_g is calculated from mean
 390 radiant temperature rather than replaced with T_a as is done for $WBGT_{in}$.

391 5 Summary and implication

392 We have developed an approximate form of WBGT that does not require iterative
 393 calculation. The need for iteration in WBGT calculation arises from the nonlinear de-
 394 pendence of mass and/or heat transfer (through convection, thermal radiation and evap-
 395 oration) efficiencies on T_g or T_{nw} , rendering the energy balance equations analytically
 396 intractable. However, we have shown that this dependence is weak for convection which
 397 is primarily influenced by wind speed. This self-dependence is also of minor importance
 398 for thermal radiation because the thermal radiative heat transfer coefficient changes by
 399 a small fraction within the typical variation range of T_g or T_{nw} , and energy loss via ther-
 400 mal radiation is much less efficient than convection and evaporation. The dependence
 401 of evaporative heat transfer coefficient on T_{nw} is of greater concern since h_{ew} is relatively
 402 sensitive to T_{nw} variations (h_{ew} varies by 2-3% per $^\circ\text{C}$ change in T_{nw}) and evaporation
 403 plays a dominant role in the energy loss of the wet wick.

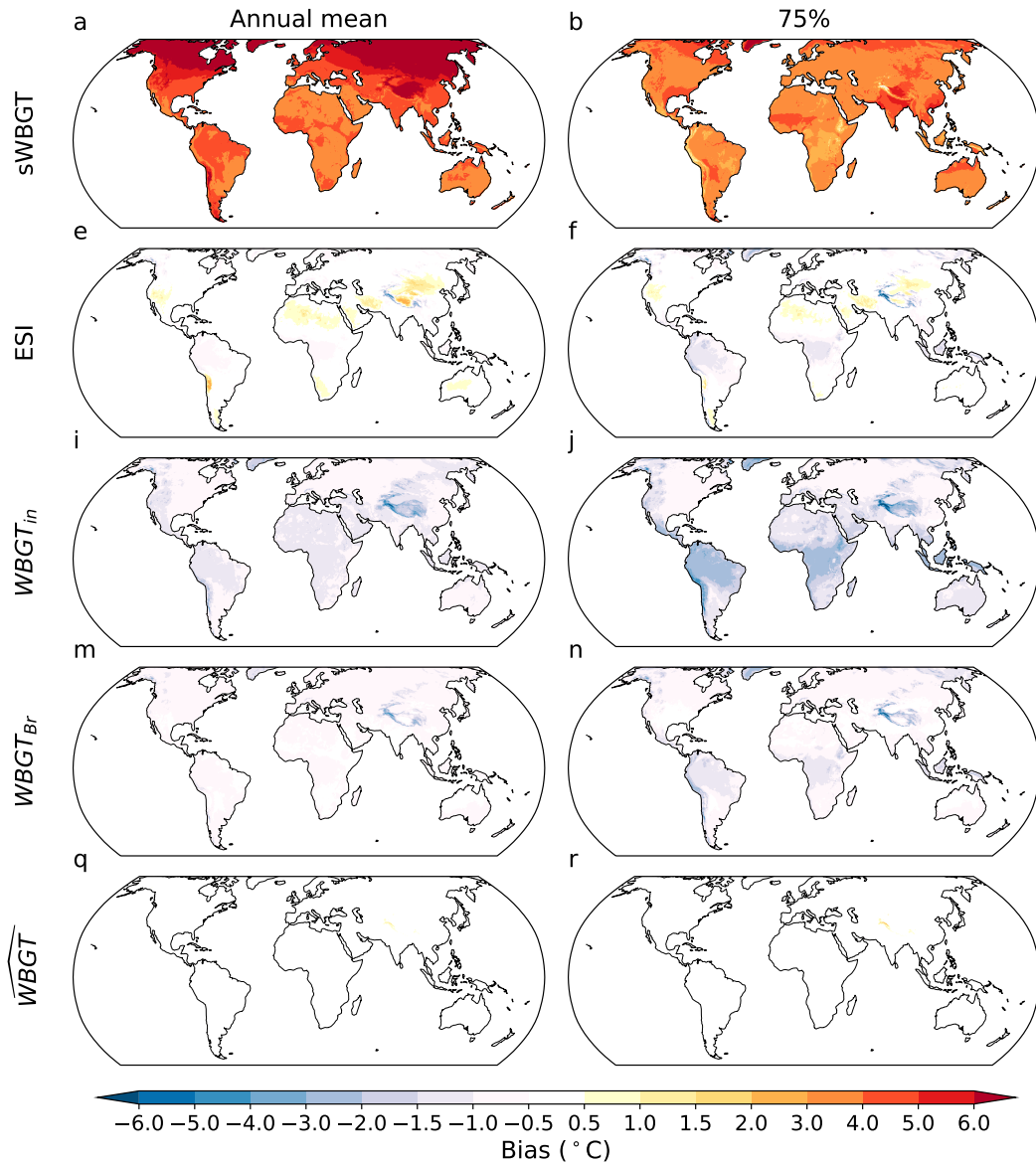


Figure 6. Biases in the annual mean and 75%, 90% and 99% percentile values of our analytic approximation (\widehat{WBGT}) and several other approximations of WBGT. Biases are evaluated by comparing against Liljegren's full model based on hourly ERA5 reanalysis data during 2013-2022.

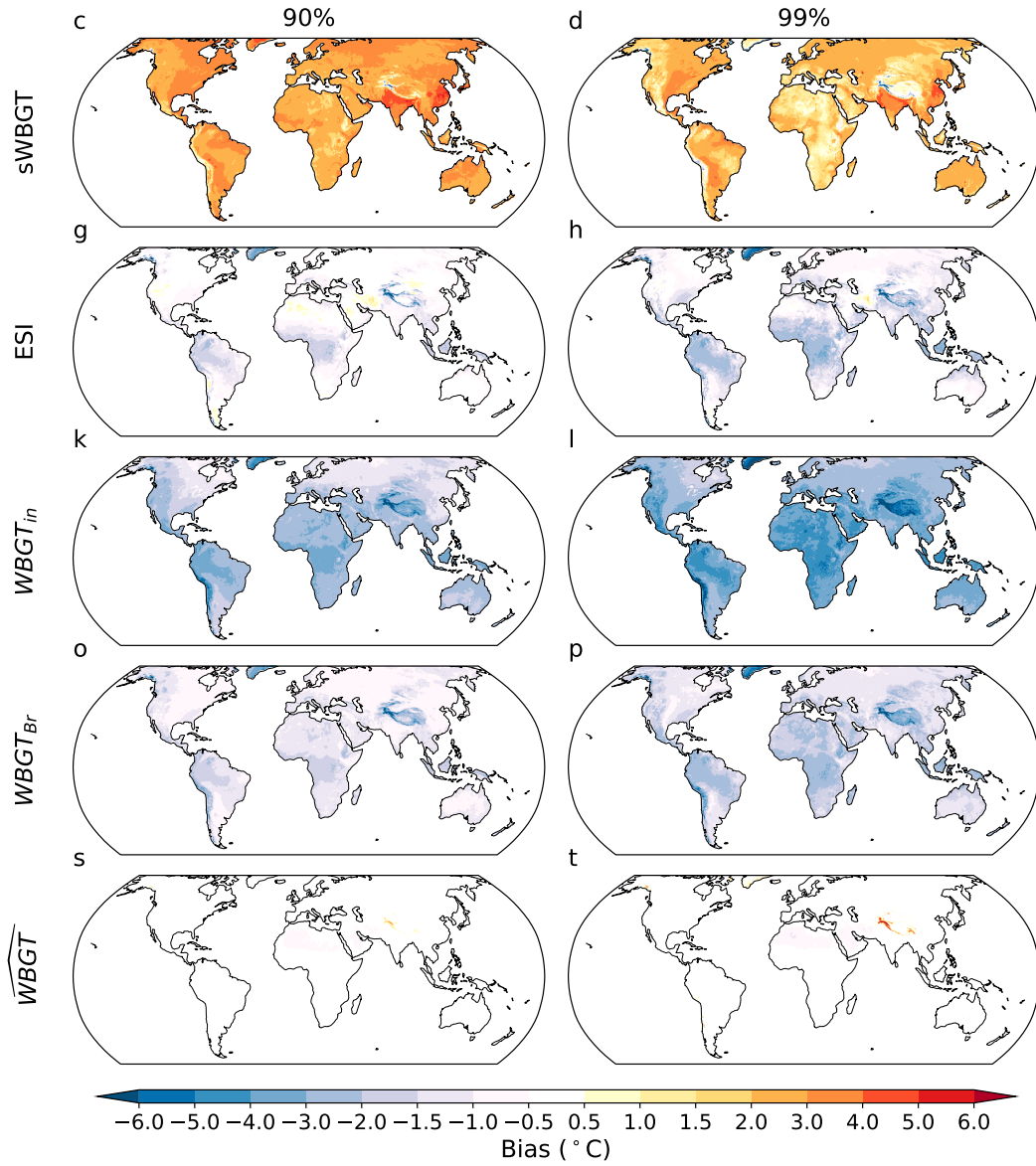


Figure 6. Continued.

404 The recognition of the weak self-nonlinearity, at least for convection and thermal
 405 radiation, motivates the development of an analytic approximation of WBGT by sub-
 406 stituting T_a and T_w as initial estimates for T_g and T_{nw} into the mass and heat transfer
 407 coefficients. The analytic approximation eliminates the need for iteration and is more
 408 accurate than other WBGT approximations commonly used in the literature. It presents
 409 an useful first guess to Liljegren's full model given its reasonably high accuracy and com-
 410 putational straightforwardness. However, users should consider the potential underes-
 411 timation of heat stress under extremely hot-dry conditions. Notably, more accurate es-
 412 timates can be obtained through a single iteration, with the analytic approximations serv-
 413 ing as the updated first guesses. Recently, Liljeren's WBGT formulation has been im-
 414 plemented into the Community Land Model Version 5 (CLM5) for non-urban settings
 415 (Buzan, 2024). Our analytic approximation could offer an useful alternative for inclu-
 416 sion in the model to prevent the model from slowing down due to iterative WBGT cal-
 417 culations.

418 The complex, nonlinear interactions between multiple meteorological parameters
 419 not only require WBGT to be calculated iteratively, but also lead to a functional form
 420 that is opaque to theoretical investigation and often times treated as a black box. As a
 421 result, WBGT—despite being a good representation of human heat stress—has not been
 422 adopted for understanding the atmospheric dynamics and thermodynamic processes contr-
 423 trolling heat stress. Instead, strictly thermodynamic variables like T_w , moist enthalpy
 424 or equivalent potential temperature are used for such purpose because of their straight-
 425 forward dynamic and thermodynamic constraint (Kong & Huber, 2023; Raymond et al.,
 426 2021; Zhang et al., 2021; Lutsko, 2021). But these thermodynamic quantities are not in-
 427 tended for or well calibrated to human heat stress which diminishes the practical rele-
 428 vance of the generated insights (Simpson et al., 2023; Lu & Romps, 2023).

429 In deriving the analytic approximation, we have gained insights that the deviation
 430 of both T_g and T_{nw} from T_a is controlled by the ratio between solar radiative heating
 431 (and VPD cooling for T_{nw}) and the efficiency of energy loss through convection and long-
 432 wave cooling (and evaporation for T_{nw}) (Eq. 4 and 8). Therefore, understanding changes
 433 in T_g , T_{nw} and consequently WBGT, must involve strong constraints or knowledge of
 434 the evolution of this ratio. Depending on the problem under consideration, if solar ra-
 435 diation and wind speed remain unchanged, the ratio for T_g (Eq. 4) is approximately con-
 436 stant given minor influence from changes in thermal radiative heat transfer efficiency.
 437 Consequently, T_g is expected to vary at the same rate as T_a . It is less straightforward
 438 to get a quick, simple relation between changes in T_{nw} and T_a , as the ratio in Eq. 8 also
 439 depends on humidity and T_{nw} itself due to the VPD cooling term and evaporative heat
 440 transfer coefficient. Nevertheless, given certain assumptions on humidity changes (e.g.,
 441 constant relative humidity), we should be able to explicitly predict how T_{nw} scales with
 442 temperature as well. In addition, since T_{nw} is driven away from T_w by solar radiation
 443 under the modulation of wind, we may expect the differences between them to be roughly
 444 constant if both solar radiation and wind remain unchanged. If this is the case, the scal-
 445 ing of T_{nw} and T_w with temperature should be close to each other.

446 More generally, Eq. 4 and Eq. 8, with their clear physical interpretation, may serve
 447 as a starting point for an analytic investigation of the sensitivity of WBGT to changes
 448 in temperature, humidity, wind and solar radiation. Clearly, we have better intuition on
 449 these traditional meteorological parameters, and established theories to constrain their
 450 variations (Zhang & Boos, 2023; Byrne, 2021; Byrne & O'Gorman, 2013, 2016; McColl
 451 & Tang, 2024). An explicit, analytic expression of WBGT's sensitivity to these tradi-
 452 tional meteorological variables helps remove the obscuring veil of WBGT's apparent com-
 453 plexity and may facilitate its application in understanding the physical control of heat
 454 stress. For example, we can quantitatively disentangle the relative role of changes in each
 455 meteorological input and the underlying physical processes in explaining WBGT responses

456 to any physical perturbations (like atmospheric blocking events, irrigation or increasing
457 greenhouse gas emission). These will be further explored in upcoming studies.

458 6 Open Research

459 Hersbach, H. et al. (2018) was downloaded from the Copernicus Climate Change
460 Service (C3S) Climate Data Store (<https://cds.climate.copernicus.eu/cdsapp#!/dataset/reanalysis-era5-single-levels?tab=form>). The results contain modified
461 Copernicus Climate Change Service information 2020. Neither the European Commis-
462 sion nor ECMWF is responsible for any use that may be made of the Copernicus infor-
463 mation or data it contains. Dix et al. (2019) was downloaded from [https://esgf-index1
464 .ceda.ac.uk/search/cmip6-ceda/](https://esgf-index1.ceda.ac.uk/search/cmip6-ceda/). Liljegren's WBGT code in C language is accessi-
465 ble at <https://github.com/mdljts/wbgt/blob/master/src/wbgt.c>, and was ported
466 to Cython (can be compiled and implemented in Python) by Kong and Huber (2022)
467 (available at <https://zenodo.org/record/5980536>). The code for the analytic WBGT
468 approximation is deposited at Zenodo (<https://zenodo.org/records/10802580>) along
469 with a Jupyter notebook to introduce its usage. The following Python packages were utilised:
470 Numpy (Harris et al., 2020), Xarray (Hoyer & Hamman, 2017), Dask (Dask Develop-
471 ment Team, 2016), Matplotlib (Hunter, 2007), and Cartopy (Met Office, 2010 - 2015).
472

473 Acknowledgments

474 This study is Funded by NASA FINESST grant 80NSSC22K1544, grant NSF 1805808-
475 CBET Innovations at the Nexus of Food, Energy, and Water Systems (INFEWS: U.S.-
476 China): A multi-scale integrated modeling approach to managing the transition to sus-
477 tainability and NSF 1829764-OAC CyberTraining: CIU:Cross-disciplinary Training for
478 Findable, Accessible, Interoperable, and Reusable (FAIR) science. We thank Rodrigo
479 Caballero for useful discussions that clarified the presentation of concepts in this study.
480 The authors declare no competing interests.

481 References

- 482 ACSM. (1984). *Position stand on the prevention of thermal injuries during distance*
483 *running* (Tech. Rep.). Medicine Sci. Sport. Exercise.
- 484 Army, U. (2003). *Heat stress control and heat casualty management* (Tech. Rep.).
485 Technical Bulletin Medical 507/Air Force Pamphlet.
- 486 Australian Bureau of Meteorology. (2010). *About the approximation to the*
487 *WBGT used by the Bureau of Meteorology*. Retrieved 2021-04-03, from
488 http://www.bom.gov.au/info/thermal_stress/#approximation
- 489 Bedingfield, C. H., & Drew, T. B. (1950). Analogy between Heat Transfer and Mass
490 Transfer. *Industrial & Engineering Chemistry*, 42(6), 1164–1173. doi: 10.1021/
491 ie50486a029
- 492 Brenda Jacklitsch, W. Jon Williams, Kristin Musolin, Aitor Coca, Jung-Hyun Kim,
493 & Nina Turner. (2016). *Criteria for a Recommended Standard: Occupational*
494 *Exposure to Heat and Hot Environments* (Tech. Rep. No. DHHS (NIOSH)
495 Publication No. 2016-106). Washington, D.C: DHHS, NIOSH.
- 496 Brimicombe, C., Lo, C. H. B., Pappenberger, F., Di Napoli, C., Maciel, P., Quintino,
497 T., . . . Cloke, H. L. (2023). Wet Bulb Globe Temperature: Indicating Extreme
498 Heat Risk on a Global Grid. *GeoHealth*, 7(2). doi: 10.1029/2022GH000701
- 499 Bröde, P., Fiala, D., Lemke, B., & Kjellstrom, T. (2018). Estimated work abil-
500 ity in warm outdoor environments depends on the chosen heat stress assess-
501 ment metric. *International Journal of Biometeorology*, 62(3), 331–345. doi:
502 10.1007/s00484-017-1346-9
- 503 Burke, M., González, F., Baylis, P., Heft-Neal, S., Baysan, C., Basu, S., &
504 Hsiang, S. (2018). Higher temperatures increase suicide rates in the

- 505 United States and Mexico. *Nature Climate Change*, 8(8), 723–729. doi:
506 10.1038/s41558-018-0222-x
- 507 Burke, M., Hsiang, S. M., & Miguel, E. (2015). Global non-linear effect of temper-
508 ature on economic production. *Nature*, 527(7577), 235–239. doi: 10.1038/
509 nature15725
- 510 Buzan, J. R. (2024). Implementation and Evaluation of Wet Bulb Globe Tempera-
511 ture Within Non-Urban Environments in the Community Land Model Version
512 5. *Journal of Advances in Modeling Earth Systems*, 16(2), e2023MS003704.
513 doi: 10.1029/2023MS003704
- 514 Buzan, J. R., & Huber, M. (2020). Moist Heat Stress on a Hotter Earth. *Annual*
515 *Review of Earth and Planetary Sciences*, 48(1), 623–655. doi: 10.1146/annurev
516 -earth-053018-060100
- 517 Buzan, J. R., Oleson, K., & Huber, M. (2015). Implementation and compari-
518 son of a suite of heat stress metrics within the Community Land Model
519 version 4.5. *Geoscientific Model Development*, 8(2), 151–170. doi:
520 10.5194/gmd-8-151-2015
- 521 Byrne, M. P. (2021). Amplified warming of extreme temperatures over tropical land.
522 *Nature Geoscience*, 14(11), 837–841. doi: 10.1038/s41561-021-00828-8
- 523 Byrne, M. P., & O’Gorman, P. A. (2013). Land–Ocean Warming Contrast
524 over a Wide Range of Climates: Convective Quasi-Equilibrium Theory
525 and Idealized Simulations. *Journal of Climate*, 26(12), 4000–4016. doi:
526 10.1175/JCLI-D-12-00262.1
- 527 Byrne, M. P., & O’Gorman, P. A. (2016). Understanding Decreases in Land Relative
528 Humidity with Global Warming: Conceptual Model and GCM Simulations.
529 *Journal of Climate*, 29(24), 9045–9061. doi: 10.1175/JCLI-D-16-0351.1
- 530 Casanueva, A., Kotlarski, S., Fischer, A. M., Flouris, A. D., Kjellstrom, T., Lemke,
531 B., ... Liniger, M. A. (2020). Escalating environmental summer heat expo-
532 sure—a future threat for the European workforce. *Regional Environmental*
533 *Change*, 20(2), 40. doi: 10.1007/s10113-020-01625-6
- 534 Chavaillaz, Y., Roy, P., Partanen, A.-I., Da Silva, L., Bresson, E., Mengis, N., ...
535 Matthews, H. D. (2019). Exposure to excessive heat and impacts on labour
536 productivity linked to cumulative CO2 emissions. *Scientific Reports*, 9(1),
537 13711. doi: 10.1038/s41598-019-50047-w
- 538 Chilton, T. H., & Colburn, A. P. (1934). Mass Transfer (Absorption) Coefficients
539 Prediction from Data on Heat Transfer and Fluid Friction. *Industrial & Engi-
540 neering Chemistry*, 26(11), 1183–1187. doi: 10.1021/ie50299a012
- 541 Clark, J., & Konrad, C. E. (2023). Observations and Estimates of Wet Bulb Globe
542 Temperature in Varied Microclimates. *Journal of Applied Meteorology and Cli-
543 matology*. doi: 10.1175/JAMC-D-23-0078.1
- 544 Dask Development Team. (2016). Dask: Library for dynamic task scheduling [Com-
545 puter software manual]. Retrieved from <https://dask.org>
- 546 de Freitas, C. R., & Grigorieva, E. A. (2015). A comprehensive catalogue and clas-
547 sification of human thermal climate indices. *International Journal of Biometeo-
548 rology*, 59(1), 109–120. doi: 10.1007/s00484-014-0819-3
- 549 de Lima, C. Z., Buzan, J. R., Moore, F. C., Baldos, U. L. C., Huber, M., & Hertel,
550 T. W. (2021). Heat stress on agricultural workers exacerbates crop impacts
551 of climate change. *Environmental Research Letters*, 16(4), 044020. doi:
552 10.1088/1748-9326/abeb9f
- 553 Dix, M., Bi, D., Dobrohotoff, P., Fiedler, R., Harman, I., Law, R., ... Yang, R.
554 (2019). *CSIRO-ARCCSS ACCESS-CM2 model output prepared for CMIP6*
555 *ScenarioMIP ssp585*. Earth System Grid Federation. Retrieved 2024-02-10,
556 from <http://cera-www.dkrz.de/WDCC/meta/CMIP6/CMIP6.ScenarioMIP>
557 .CSIRO-ARCCSS.ACCESS-CM2.ssp585 (Medium: application/x-netcdf Version
558 Number: 20230220 Type: dataset) doi: 10.22033/ESGF/CMIP6.4332
- 559 Dunne, J. P., Stouffer, R. J., & John, J. G. (2013). Reductions in labour capacity

- 560 from heat stress under climate warming. *Nature Climate Change*, 3(6), 563–
561 566. doi: 10.1038/nclimate1827
- 562 Ebi, K. L., Capon, A., Berry, P., Broderick, C., De Dear, R., Havenith, G., ...
563 Jay, O. (2021). Hot weather and heat extremes: health risks. *The Lancet*,
564 398(10301), 698–708. doi: 10.1016/S0140-6736(21)01208-3
- 565 Foster, J., Smallcombe, J. W., Hodder, S., Jay, O., Flouris, A. D., & Havenith, G.
566 (2022). Quantifying the impact of heat on human physical work capacity; part
567 II: the observed interaction of air velocity with temperature, humidity, sweat
568 rate, and clothing is not captured by most heat stress indices. *International*
569 *Journal of Biometeorology*, 66(3), 507–520. doi: 10.1007/s00484-021-02212-y
- 570 Foster, J., Smallcombe, J. W., Hodder, S., Jay, O., Flouris, A. D., Nybo, L., &
571 Havenith, G. (2022). Quantifying the impact of heat on human physical work
572 capacity; part III: the impact of solar radiation varies with air temperature,
573 humidity, and clothing coverage. *International Journal of Biometeorology*,
574 66(1), 175–188. doi: 10.1007/s00484-021-02205-x
- 575 Gao, J., Wang, Y., Wu, X., Gu, X., & Song, X. (2019). A simplified indoor wet-bulb
576 globe temperature formula to determine acceptable hot environmental paramet-
577 ers in naturally ventilated buildings. *Energy and Buildings*, 196, 169–177. doi:
578 10.1016/j.enbuild.2019.05.035
- 579 Harris, C. R., Millman, K. J., van der Walt, S. J., Gommers, R., Virtanen, P., Cour-
580 napeau, D., ... Oliphant, T. E. (2020). Array programming with NumPy.
581 *Nature*, 585(7825), 357–362. doi: 10.1038/s41586-020-2649-2
- 582 Hausfather, Z. (2019). *Cmip6: The next generation of climate models ex-*
583 *plained*. Retrieved 2024-02-13, from [https://www.carbonbrief.org/
584 cmip6-the-next-generation-of-climate-models-explained](https://www.carbonbrief.org/cmip6-the-next-generation-of-climate-models-explained)
- 585 Havenith, G., & Fiala, D. (2015, December). Thermal Indices and Thermophysiol-
586 ogical Modeling for Heat Stress. In R. Terjung (Ed.), *Comprehensive Physiology*
587 (pp. 255–302). Hoboken, NJ, USA: John Wiley & Sons, Inc. Retrieved 2020-
588 06-27, from <http://doi.wiley.com/10.1002/cphy.c140051> doi: 10.1002/
589 cphy.c140051
- 590 Hersbach, H., Bell, B., Berrisford, P., Biavati, G., Horányi, A., Muñoz Sabater, J.,
591 ... Thépaut, J.-N. (2018). ERA5 hourly data on single levels from 1979 to
592 present. *Copernicus Climate Change Service (C3S) Climate Data Store (CDS)*.
593 doi: 10.24381/cds.adbb2d47
- 594 Hoyer, S., & Hamman, J. (2017). xarray: N-D labeled arrays and datasets in
595 Python. *Journal of Open Research Software*, 5(1). doi: 10.5334/jors.148
- 596 Hsiang, S. M., Burke, M., & Miguel, E. (2013). Quantifying the Influence of Cli-
597 mate on Human Conflict. *Science*, 341(6151), 1235367. doi: 10.1126/science
598 .1235367
- 599 Hunter, J. D. (2007). Matplotlib: A 2d graphics environment. *Computing in Science*
600 *& Engineering*, 9(3), 90–95. doi: 10.1109/MCSE.2007.55
- 601 Ioannou, L. G., Tsoutsoubi, L., Mantzios, K., Vliora, M., Nintou, E., Piil, J. F., ...
602 Flouris, A. D. (2022). Indicators to assess physiological heat strain – Part 3:
603 Multi-country field evaluation and consensus recommendations. *Temperature*,
604 9(3), 274–291. doi: 10.1080/23328940.2022.2044739
- 605 ISO. (1998). *Ergonomics of the thermal environment - instruments for measuring*
606 *physical quantities* (International Standard). Geneva: International Organiza-
607 tion for Standardization (ISO).
- 608 ISO. (2017). *Ergonomics of the thermal environment — Assessment of heat stress*
609 *using the WBGT (wet bulb globe temperature) index* (International Standard).
610 Geneva: International Organization for Standardization (ISO).
- 611 Kamal, A. S. M. M., Faruki Fahim, A. K., & Shahid, S. (2024). Simplified equations
612 for wet bulb globe temperature estimation in Bangladesh. *International Jour-*
613 *nal of Climatology*, joc.8402. doi: 10.1002/joc.8402
- 614 Kjellstrom, T., Briggs, D., Freyberg, C., Lemke, B., Otto, M., & Hyatt, O. (2016).

- 615 Heat, Human Performance, and Occupational Health: A Key Issue for the As-
 616 sessment of Global Climate Change Impacts. *Annual Review of Public Health*,
 617 37(1), 97–112. doi: 10.1146/annurev-publhealth-032315-021740
- 618 Kjellstrom, T., Freyberg, C., Lemke, B., Otto, M., & Briggs, D. (2018). Estimating
 619 population heat exposure and impacts on working people in conjunction with
 620 climate change. *International Journal of Biometeorology*, 62(3), 291–306. doi:
 621 10.1007/s00484-017-1407-0
- 622 Kong, Q., & Huber, M. (2022). Explicit calculations of Wet Bulb Globe Tempera-
 623 ture compared with approximations and why it matters for labor productivity.
 624 *Earth's Future*. doi: 10.1029/2021EF002334
- 625 Kong, Q., & Huber, M. (2023). Regimes of soil moisture-wet bulb temperature cou-
 626 pling with relevance to moist heat stress. *Journal of Climate*, 1–45. doi: 10
 627 .1175/JCLI-D-23-0132.1
- 628 Lemke, B., & Kjellstrom, T. (2012). Calculating workplace WBGT from meteorolog-
 629 ical data: a tool for climate change assessment. *Industrial Health*, 50(4), 267–
 630 278. doi: 10.2486/indhealth.MS1352
- 631 Li, C., Sun, Y., Zwiers, F., Wang, D., Zhang, X., Chen, G., & Wu, H. (2020).
 632 Rapid Warming in Summer Wet Bulb Globe Temperature in China with
 633 Human-Induced Climate Change. *Journal of Climate*, 33(13), 5697–5711. doi:
 634 10.1175/JCLI-D-19-0492.1
- 635 Li, D., Yuan, J., & Kopp, R. E. (2020). Escalating global exposure to compound
 636 heat-humidity extremes with warming. *Environmental Research Letters*, 15(6),
 637 064003. doi: 10.1088/1748-9326/ab7d04
- 638 Liljegren, J. C., Carhart, R. A., Lawday, P., Tschopp, S., & Sharp, R. (2008).
 639 Modeling the Wet Bulb Globe Temperature Using Standard Meteorological
 640 Measurements. *Journal of Occupational and Environmental Hygiene*, 5(10),
 641 645–655. doi: 10.1080/15459620802310770
- 642 Lu, Y.-C., & Romps, D. (2023). Wet-Bulb Temperature or Heat Index: Which Bet-
 643 ter Predicts Fatal Heat in a Warming Climate? *Physiology*, 38(S1), 5734524.
 644 doi: 10.1152/physiol.2023.38.S1.5734524
- 645 Lutsko, N. J. (2021). The Relative Contributions of Temperature and Moisture to
 646 Heat Stress Changes under Warming. *Journal of Climate*, 34(3), 901–917. doi:
 647 10.1175/JCLI-D-20-0262.1
- 648 Matsumoto, K., Tachiiri, K., & Su, X. (2021). Heat stress, labor productivity, and
 649 economic impacts: analysis of climate change impacts using two-way coupled
 650 modeling. *Environmental Research Communications*, 3(12), 125001. doi:
 651 10.1088/2515-7620/ac3e14
- 652 McColl, K. A., & Tang, L. I. (2024). An Analytic Theory of Near-Surface Relative
 653 Humidity over Land. *Journal of Climate*, 37(4), 1213–1230. doi: 10.1175/JCLI
 654 -D-23-0342.1
- 655 Met Office. (2010 - 2015). Cartopy: a cartographic python library with a mat-
 656 plotlib interface [Computer software manual]. Exeter, Devon. Retrieved from
 657 <https://scitools.org.uk/cartopy>
- 658 Moran, D., Pandolf, K., Shapiro, Y., Heled, Y., Shani, Y., Mathew, W., & Gonza-
 659 lez, R. (2001). An environmental stress index (ESI) as a substitute for the
 660 wet bulb globe temperature (WBGT). *Journal of Thermal Biology*, 26(4-5),
 661 427–431. doi: 10.1016/S0306-4565(01)00055-9
- 662 NIOSH. (2016). *Criteria for a Recommended Standard: Occupational Exposure to*
 663 *Heat and Hot Environments* (Tech. Rep. No. DHHS (NIOSH) Publication No.
 664 2016-106). Washington, D.C: DHHS, NIOSH.
- 665 Orlov, A., De Hertog, S., Havermann, F., Guo, S., Luo, F., Manola, I., . . . Schleuss-
 666 ner, C. (2023). Changes in Land Cover and Management Affect Heat
 667 Stress and Labor Capacity. *Earth's Future*, 11(3), e2022EF002909. doi:
 668 10.1029/2022EF002909
- 669 OSHA. (2017). *Osha technical manual, section iii, chapter 4:heat stress*. (Tech. Rep.

- 670 No. TED-01-00-015). Washington (DC): U.S. Department of Labor, OSHA:
 671 Occupational Safety and Health Administration (OSHA).
- 672 Patel, T., Mullen, S. P., & Santee, W. R. (2013). Comparison of Methods
 673 for Estimating Wet-Bulb Globe Temperature Index From Standard Me-
 674 teorological Measurements. *Military Medicine*, *178*(8), 926–933. doi:
 675 10.7205/MILMED-D-13-00117
- 676 Raymond, C., Matthews, T., Horton, R. M., Fischer, E. M., Fueglistaler, S.,
 677 Ivanovich, C., ... Zhang, Y. (2021). On the Controlling Factors for Glob-
 678 ally Extreme Humid Heat. *Geophysical Research Letters*, *48*(23). doi:
 679 10.1029/2021GL096082
- 680 Saeed, W., Haqiqi, I., Kong, Q., Huber, M., Buzan, J. R., Chonabayashi, S.,
 681 ... Hertel, T. W. (2022). The Poverty Impacts of Labor Heat Stress
 682 in West Africa Under a Warming Climate. *Earth's Future*, *10*(11). doi:
 683 10.1029/2022EF002777
- 684 Sherwood, S. C., & Huber, M. (2010). An adaptability limit to climate change
 685 due to heat stress. *Proceedings of the National Academy of Sciences*, *107*(21),
 686 9552–9555. doi: 10.1073/pnas.0913352107
- 687 Simpson, C. H., Brousse, O., Ebi, K. L., & Heaviside, C. (2023). Commonly used in-
 688 dices disagree about the effect of moisture on heat stress. *npj Climate and At-
 689 mospheric Science*, *6*(1), 78. doi: 10.1038/s41612-023-00408-0
- 690 Stull, R. (2011). Wet-Bulb Temperature from Relative Humidity and Air Tempera-
 691 ture. *Journal of Applied Meteorology and Climatology*, *50*(11), 2267–2269. doi:
 692 10.1175/JAMC-D-11-0143.1
- 693 Tuholske, C., Caylor, K., Funk, C., Verdin, A., Sweeney, S., Grace, K., ... Evans,
 694 T. (2021, October). Global urban population exposure to extreme heat. *Pro-
 695 ceedings of the National Academy of Sciences*, *118*(41), e2024792118. doi:
 696 10.1073/pnas.2024792118
- 697 Vecellio, D. J., Wolf, S. T., Cottle, R. M., & Kenney, W. L. (2022). Utility of the
 698 Heat Index in defining the upper limits of thermal balance during light phys-
 699 ical activity (PSU HEAT Project). *International Journal of Biometeorology*,
 700 *66*(9), 1759–1769. doi: 10.1007/s00484-022-02316-z
- 701 Williams, I. N., Pierrehumbert, R. T., & Huber, M. (2009). Global warming, con-
 702 vective threshold and false thermostats. *Geophysical Research Letters*, *36*(21),
 703 L21805. doi: 10.1029/2009GL039849
- 704 Yaglou, C. P., & Minard, D. (1957). Control of heat casualties at military training
 705 centers. *A.M.A. archives of industrial health*, *16*(4), 302–316.
- 706 Zhang, Y., & Boos, W. R. (2023). An upper bound for extreme temperatures over
 707 midlatitude land. *Proceedings of the National Academy of Sciences*, *120*(12),
 708 e2215278120. doi: 10.1073/pnas.2215278120
- 709 Zhang, Y., Held, I., & Fueglistaler, S. (2021). Projections of tropical heat stress con-
 710 strained by atmospheric dynamics. *Nature Geoscience*, *14*(3), 133–137. doi: 10
 711 .1038/s41561-021-00695-3
- 712 Zhang, Y., & Shindell, D. T. (2021). Costs from labor losses due to extreme heat in
 713 the USA attributable to climate change. *Climatic Change*, *164*(3-4), 35. doi:
 714 10.1007/s10584-021-03014-2
- 715 Zhu, J., Wang, S., Zhang, B., & Wang, D. (2021). Adapting to Changing Labor Pro-
 716 ductivity as a Result of Intensified Heat Stress in a Changing Climate. *Geo-
 717 Health*, *5*(4). doi: 10.1029/2020GH000313

Abstract

Wet-bulb globe temperature (WBGT)—a standard measure for workplace heat stress regulation—incorporates the complex, nonlinear interaction among temperature, humidity, wind and radiation. This complexity requires WBGT to be calculated iteratively following the recommended approach developed by Liljegren and colleagues. The need for iteration has limited the wide application of Liljegren’s approach, and stimulated various simplified WBGT approximations that do not require iteration but are potentially seriously biased. By carefully examining the self-nonlinearities in Liljegren’s model, we develop a zero-iteration analytic approximation of WBGT while maintaining sufficient accuracy and the physical basis of the original model. The new approximation slightly deviates from Liljegren’s full model—by less than 1°C in 99% cases over 93% of global land area. The annual mean and 75-99% percentiles of WBGT are also well represented with biases within $\pm 0.5^\circ\text{C}$ globally. This approximation is clearly more accurate than other commonly used WBGT approximations. Physical intuition can be developed on the processes controlling WBGT variations from an energy balance perspective. This may provide a basis for applying WBGT to understanding the physical control of heat stress.

Plain Language Summary

Wet-bulb globe temperature (WBGT) is a standard way to measure heat stress in the workplace. It incorporates the complex, nonlinear interactive effects of temperature, humidity, wind and radiation. This complexity requires WBGT to be calculated iteratively which is computationally intensive and less straightforward to implement algorithmically. To address these issues, we came up with a simplified version of WBGT that obviates the need for iteration. This simplified approach is computationally straightforward and also highly accurate.

1 Introduction

Heat stress presents significant threats to human health (Ebi et al., 2021; Buzan & Huber, 2020; Kjellstrom et al., 2016) with wide-ranging social (Hsiang et al., 2013; Burke et al., 2018) and economic consequences (Burke et al., 2015; Saeed et al., 2022). Metrics that accurately represent the physiological impact of heat stress are crucial for the monitoring, early warning, and impact assessment of heat stress (Havenith & Fiala, 2015; Simpson et al., 2023). Over the last century, numerous heat stress metrics have been formulated (de Freitas & Grigorieva, 2015), among which the wet-bulb globe temperature (WBGT) emerges as a notably comprehensive measure, encapsulating the interplay of temperature, humidity, wind speed and radiation effects (Yaglou & Minard, 1957). Rooted in physiology principles and fortified by empirical calibration, WBGT is as good or better than most other metrics in predicting human heat stress compensability (Vecellio et al., 2022), assessing the physiological influences of heat stress (Ioannou et al., 2022), and capturing the interactive effects of multiple meteorological factors on human physical work capacity (Foster et al., 2022, 2022). It has been incorporated into several heat stress regulatory standards across various domains including occupational health (NIOSH, 2016; ISO, 2017; OSHA, 2017), military operations (Army, 2003) and athletic activities (ACSM, 1984).

WBGT is defined as

$$WBGT = 0.7T_{nw} + 0.2T_g + 0.1T_a \quad (1)$$

under outdoor conditions where T_{nw} , T_g and T_a refer to natural wet-bulb temperature, black globe temperature and dry-bulb temperature respectively. The WBGT model developed by Liljegren et al. (2008) is the recommended approach for WBGT calculation due to its foundation on heat and mass transfer principles, careful treatment of the geometry of WBGT sensors, and extensive validation (RMSE < 1°C) (Liljegren et al., 2008;

62 Lemke & Kjellstrom, 2012; Patel et al., 2013; Clark & Konrad, 2023). It derives T_{nw} and
 63 T_g by solving the nonlinear energy balance equations of the wet wick and black globe
 64 sensors. However, this process requires iterative calculations which have limited the widespread
 65 adoption of Liljegren’s approach. Even in recent work, a preference for simpler WBGT
 66 approximations that avoid iteration persists within the scientific community (e.g., Zhu
 67 et al. (2021); Brimicombe et al. (2023); Tuholske et al. (2021); Orlov et al. (2023); Kamal
 68 et al. (2024)). However, these simplified approximations are so diverse in formulation that
 69 they generate substantially different estimates making the results from different stud-
 70 ies challenging to meaningfully compare (Lemke & Kjellstrom, 2012; Kong & Huber, 2022).
 71 Some approximations are based on statistical relationship rather than physics (Moran
 72 et al., 2001; Australian Bureau of Meteorology, 2010; Kamal et al., 2024). The Australian
 73 Bureau of Meteorology WBGT formulation (hereafter referred as *sWBGT*) (Australian
 74 Bureau of Meteorology, 2010) has been demonstrated to be systematically biased, but
 75 remain widely used because of their simplicity (Kong & Huber, 2022). The generated
 76 heat stress estimates have been fed into impact models for assessing downstream social-
 77 economic consequences (Zhang & Shindell, 2021; Chavillaz et al., 2019; Zhu et al., 2021;
 78 Matsumoto et al., 2021; de Lima et al., 2021). The propagation of biases stemming from
 79 these WBGT approximations through the chain of climate change impact assessment could
 80 potentially mislead policy-making pertaining to heat stress mitigation and adaptation.

81 We aim to address this issue by developing a simplified WBGT model that does
 82 not require iteration while maintaining sufficient accuracy and physics of heat and mass
 83 transfer. This is achieved with an analytic approximation of Liljegren’s WBGT through
 84 substituting reasonable first-guess values of T_{nw} and T_g into the energy balance equa-
 85 tions of the wet wick and black globe sensors. The analytic approximation will be eval-
 86 uated against Liljegren’s full model which, although subject to biases compared to field
 87 observations (Lemke & Kjellstrom, 2012; Patel et al., 2013; Liljegren et al., 2008; Clark
 88 & Konrad, 2023), is treated as ground truth in this paper.

89 The remainder of this paper is structured as follows. Section 2 provides a concise
 90 overview of Liljegren’s WBGT model focusing on the nonlinear energy balance equations.
 91 Section 3 introduces the analytic approximation of WBGT the accuracy of which is eval-
 92 uated in Section 4. This evaluation is first conducted with synthetic data to understand
 93 the bias structure across the multidimensional parameter space encompassing temper-
 94 ature, humidity, solar radiation and wind speed (Section 4.1). We then explore the mag-
 95 nitude and spatial distribution of biases within a more realistic context (Section 4.2). This
 96 is primarily done with ERA5 reanalysis (Hersbach, H. et al., 2018) for a historical pe-
 97 riod, supplemented by the ACCESS-CM2 model (Dix et al., 2019) for a warmer climate.
 98 Afterwards, we compare this analytic approximation against other commonly used ap-
 99 proximations of WBGT (Section 4.3). Section 5 contains a brief summary and implica-
 100 tions on applying WBGT to understanding physical processes controlling heat stress.

101 2 Liljegren WBGT model

102 Here we briefly review the T_g and T_{nw} formulations in Liljegren’s WBGT model
 103 while directing interested readers to Liljegren et al. (2008) and Kong and Huber (2022)
 104 for details.

105 2.1 Black globe temperature

106 The energy balance equation for the black globe is given by

$$\sigma\epsilon_g T_g^4 + h_{cg}(T_g - T_a) = LR_g + SR_g \quad (2)$$

107 where energy gain from incoming thermal (LR_g) and solar radiation (SR_g) is balanced
 108 by long-wave cooling and energy loss through convective heat transfer between the globe
 109 and ambient air corresponding respectively to the two terms on the left side of Eq. 2.

110 Note that LR_g encompasses both downward and upwelling thermal radiation; SR_g also
 111 integrates heating from both downward (direct and diffuse) and ground surface reflected
 112 solar radiation, and incorporates parameters representing solar zenith angle, albedo of
 113 the globe and ground surface, and globe geometry characteristics. Please refer to Liljegren
 114 et al. (2008) and Kong and Huber (2022) for the formulations of LR_g and SR_g . h_{cg} sig-
 115 nifies convective heat transfer coefficient associated with the globe; σ and ϵ_g stand for
 116 the Stefan-Boltzmann constant and emissivity of the globe. Eq. 2 is analogous to to Eq.
 117 15 in Liljegren et al. (2008), although the long-wave and surface reflected short-wave ra-
 118 diation embedded within LR_g and SR_g will be obtained directly from climate model out-
 119 put as was done in Kong and Huber (2022). In Liljegren's original approach, these ra-
 120 diative fluxes are approximated from temperature, humidity and ground surface albedo.

121 Eq. 2 can be rearranged into

$$T_g = T_a + \frac{SR_g + LR_g - \sigma\epsilon_g T_a^4}{h_{cg} + h_{rg}} \quad (3)$$

122 where h_{rg} can be interpreted as a thermal radiative heat transfer coefficient

$$h_{rg} = \sigma\epsilon_g(T_g^2 + T_a^2)(T_g + T_a)$$

123 Note that $LR_g - \sigma\epsilon_g T_a^4$ is typically small and actually approaches zero when the
 124 downward and upward thermal radiation can be represented by a mean radiant temper-
 125 ature of T_a in absence of solar radiation. With this term being neglected, we have

$$T_g - T_a = \frac{SR_g}{h_{cg} + h_{rg}} \quad (4)$$

126 The physical interpretation of Eq. 4 is that the efficiency of energy loss through
 127 long-wave cooling (h_{rg}) and convection (h_{cg}) modulates the required temperature gra-
 128 dient between the globe and ambient air in order to balance the energy gain from solar
 129 radiation.

130 Eq. 3 cannot be solved analytically since both h_{cg} and h_{rg} depend nonlinearly on
 131 T_g (i.e., Eq. 3 is self-nonlinear in T_g). h_{cg} is derived from the empirical correlation for
 132 heat transfer from a sphere in cross flow (Brenda Jacklitsch et al., 2016) (see Eq. 16 in
 133 Liljegren et al. (2008) for its formulation). It is mainly affected by wind speed but also
 134 depends on film temperature (T_f) which is the temperature of the air within the con-
 135 vective boundary layer proximate to the surface of the globe, and is calculated as the
 136 arithmetic mean between the temperatures of the globe surface and ambient air ($T_f =$
 137 $(T_g + T_a)/2$). Consequently, Eq. 3 needs to be solved by iteration to obtain the equi-
 138 librium T_g . In Section 3.1, we will provide an analytic solution to T_g which does not re-
 139 quire iteration.

140 2.2 Natural wet-bulb temperature

141 The energy balance equation for the wick is

$$k_x \frac{e_w - e_a}{P - e_w} M_{H_2O} \Delta H + h_{cw}(T_{nw} - T_a) + \sigma\epsilon_w T_{nw}^4 = LR_w + SR_w \quad (5)$$

142 where the radiative energy gain on the right side of the equation is balanced by en-
 143 ergy loss through evaporating water, convection, and thermal radiation corresponding
 144 respectively to the three terms on the left side of the equation. The convective heat trans-
 145 fer coefficient h_{cw} is obtained from the empirical correlation for heat transfer from a cylin-
 146 der (Bedingfield & Drew, 1950). k_x denotes convective mass transfer coefficient which
 147 are interconnected with h_{cw} via the Chilton-Colburn analogy (Chilton & Colburn, 1934).

148 They are both predominantly affected by wind speed with weak dependence on film tem-
 149 perature ($T_f = (T_a + T_{nw})/2$) (see Eq. 8 and 10 in Liljegren et al. (2008) for their for-
 150 mulations). e_a and e_w represent ambient vapor pressure and the saturation vapor pres-
 151 sure at the temperature of the wick ($e_w = e_{sat}(T_{nw})$); P is surface pressure; M_{H_2O} is
 152 the molecular weight of water vapor; ΔH stands for the heat of vaporization.

153 Eq. 5 can be rearranged into

$$T_{nw} = T_a + \frac{SR_w - \beta(e_{sat}(T_a) - e_a) + LR_w - \sigma\epsilon_w T_a^4}{h_{ew} + h_{cw} + h_{rw}} \quad (6)$$

154 where β is defined as

$$\beta = \frac{k_x M_{H_2O} \Delta H}{P - e_w} \approx \frac{k_x M_{H_2O} \Delta H}{P}$$

155 h_{ew} and h_{rw} can be interpreted as evaporative and thermal radiative heat trans-
 156 fer coefficients for the wick cylinder, and are defined as

$$h_{ew} = \beta \frac{e_w - e_{sat}(T_a)}{T_{nw} - T_a} \approx \beta \left. \frac{\partial e_{sat}(T)}{\partial T} \right|_{T = \frac{T_{nw} + T_a}{2}} \quad (7)$$

157

$$h_{rw} = \sigma\epsilon_w (T_{nw}^2 + T_a^2)(T_{nw} + T_a)$$

158 Note that h_{ew} , by definition, measures the efficiency of evaporative heat transfer
 159 between the wet wick and a saturated air. The fact that air can be under-saturated cre-
 160 ates a cooling term from vapor pressure deficit (VPD) ($\beta(e_{sat}(T_a) - e_a)$ in Eq. 6).

161 With $LR_w - \sigma\epsilon_w T_a^4$ being typically small and neglected, we have

$$T_{nw} - T_a = \frac{SR_w - \beta(e_{sat}(T_a) - e_a)}{h_{ew} + h_{cw} + h_{rw}} \quad (8)$$

162 Namely, the temperature gradient between the wick and ambient air is driven by net en-
 163 ergy input from solar radiation and VPD, regulated by the efficiency of energy loss via
 164 evaporation (h_{ew}), convection (h_{cw}) and long-wave cooling (h_{rw}).

165 Similar to the case of T_g , Eq. 6 needs to be solved by iteration because both the
 166 mass transfer (k_x) and three heat transfer coefficients (h_{ew} , h_{cw} and h_{rw}) depend non-
 167 linearly on T_{nw} . An analytic approximation to T_{nw} will be provided in Section 3.2 by
 168 removing the self-nonlinearity.

169 3 Analytic approximation of wet-bulb globe temperature

170 In the previous section, we established that both T_g and T_{nw} cannot be solved an-
 171alytically because they are embedded nonlinearly within the mass and heat transfer co-
 172efficients. Numerical solutions can be pursued through iterative methods: starting with
 173an initial guess, inserting it into the transfer coefficients within Eq. 3 or 6, obtaining an
 174updated value, and iteratively repeating this process until consecutive updates deviate
 175by less than a specified tolerance. However, we argue that employing a judicious initial
 176guess might yield a result that is sufficiently accurate, thereby eliminating the need for
 177iterations. By employing this approach, Eq. 3 and 6 become analytic formulations of T_g
 178and T_{nw} , and the ensuing solutions are henceforth referred to as analytic approximations.

179 3.1 Black globe temperature

180 An analytic approximation of T_g can be obtained by substituting a certain first-
 181guess value of T_g into h_{cg} and h_{rg} on the right side of Eq. 3. Ideally, the first-guess value
 182should be close to T_g , but this is less critical due to reasons articulated below.

183 h_{cg} is derived from empirical correlations under forced convection with surround-
 184 ing fluid motion (Liljegren et al., 2008), and therefore is primarily dictated by wind speed
 185 with minimal sensitivity to film temperature (Fig. 1a and d). This choice is justified by
 186 the dominance of forced convection over free convection under non-negligible wind speeds
 187 and reasonable temperature gradients between the globe and ambient air (Gao et al.,
 188 2019). Under a wind speed of 2 m/s, a 10 °C increase of film temperature from 30 to 40
 189 °C only cause a 0.2% reduction in h_{cg} (Fig. 1d). In fact, the international standard ISO
 190 7726 (ISO, 1998) parameterizes convective heat transfer coefficients under forced con-
 191 vection as solely a function of wind speed. On the other hand, h_{rg} only varies by around
 192 0.5% per °C change in T_g , and energy loss via thermal radiation is typically 2-5 times
 193 less efficient than convection (Fig. 1a).

194 The minor influence of temperature on h_{cg} and small fractional changes in h_{rg} with
 195 temperature suggest that the initial estimate's proximity to the true value is not crit-
 196 ical. Therefore, we choose T_a as a first guess for T_g for simplicity. The resultant approx-
 197 imations to both heat transfer coefficients are denoted as \widehat{h}_{cg} and \widehat{h}_{rg} the latter of which
 198 is calculated as $\widehat{h}_{rg} = 4\sigma\epsilon_g T_a^3$. For \widehat{h}_{cg} , film temperature is approximated by $T_f = \frac{T_g + T_a}{2} \approx$
 199 T_a . Consequently, we have an analytic approximation of T_g :

$$\widehat{T}_g = T_a + \frac{SR_g + LR_g - \sigma\epsilon_g T_a^4}{\widehat{h}_{cg} + \widehat{h}_{rg}} \quad (9)$$

200 The accuracy of \widehat{T}_g can be assessed by comparing it against the true value of T_g in Eq.
 201 3.

$$\widehat{T}_g - T_g = (T_g - T_a) \frac{h_{cg} - \widehat{h}_{cg} + h_{rg} - \widehat{h}_{rg}}{\widehat{h}_{cg} + \widehat{h}_{rg}}$$

202 As explained above, the deviation of \widehat{h}_{cg} from h_{cg} is negligible, which simplifies the
 203 bias of \widehat{T}_g into

$$\begin{aligned} \widehat{T}_g - T_g &= (T_g - T_a) \frac{h_{rg} - \widehat{h}_{rg}}{\widehat{h}_{cg} + \widehat{h}_{rg}} \\ &= \frac{\sigma\epsilon_g (T_g - T_a)^2 [(T_g + T_a)^2 + 2T_a^2]}{\widehat{h}_{cg} + \widehat{h}_{rg}} \end{aligned} \quad (10)$$

204 It is clear that \widehat{T}_g always has non-negative biases the magnitude of which is proportional
 205 to the square of the temperature gradient between the globe and ambient air. There-
 206 fore, \widehat{T}_g is expected to perform better under conditions of weak solar radiation and high
 207 wind speed wherein the weaker solar heating and efficient convective heat transfer make
 208 T_g closer to T_a . Given T_g and T_a of $\sim 300\text{K}$ and $T_g - T_a$ of $\sim 20\text{K}$, the largest possible
 209 bias is $\sim 2\text{K}$ which can only be realized when $h_{cg} = 0$. However, the actual bias will be
 210 significantly smaller since h_{cg} is usually considerably larger than h_{rg} (Fig. 1a). The phys-
 211 ical interpretation of this formulation is that the approximation to long-wave cooling in-
 212 troduces minimal biases when convection is the dominant pathway for energy loss.

213 3.2 Natural wet-bulb temperature

214 An analytic solution for T_{nw} can be obtained by substituting a first-guess value of
 215 T_{nw} into the mass and three heat transfer coefficients in Eq. 6. Similar to the case of
 216 T_g , both k_x and h_{cw} exhibit minimal sensitivity to temperature variations (Fig. 1b-d).
 217 h_{rw} only varies by 0.5% per °C change in T_{nw} and energy loss via thermal radiation is
 218 much less efficient than convection and evaporation (Fig. 1b). Therefore, the proxim-
 219 ity of the first guess to the true T_{nw} is less critical for mass transfer and heat transfer

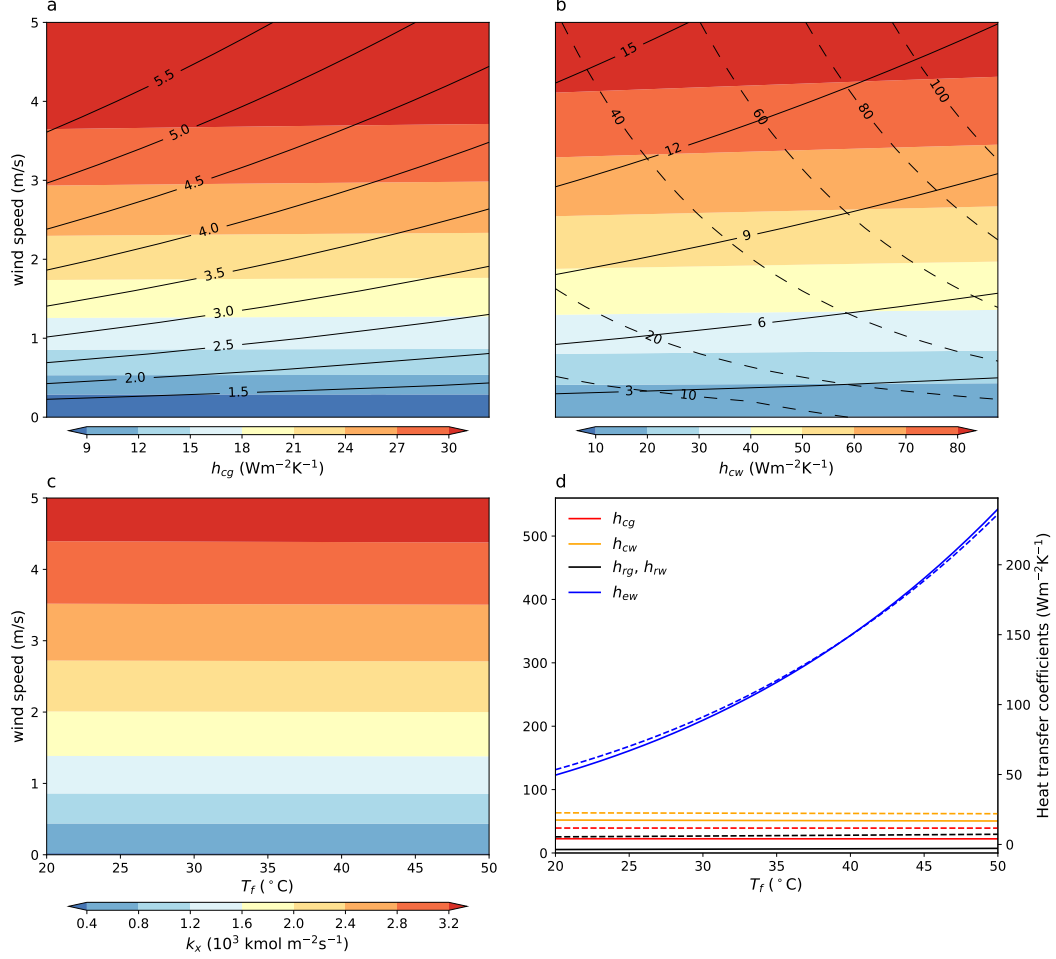


Figure 1. Shadings in (a)-(c) denote h_{cg} , h_{cw} and k_x respectively. Solid contours in (a) and (b) represent the ratio between convective and thermal radiative heat transfer coefficients for the black globe (h_{cg}/h_{rg}) and wick cylinder (h_{cw}/h_{rw}). Dashed contours in (b) represent the ratio between h_{ew} and h_{rw} . Values in panel (a)-(c) are expressed as functions of film temperature and wind speed. (d) Various heat transfer coefficients for the globe and wick as functions of film temperature under a 2m/s (solid lines corresponding to left y-axis) and 0.5m/s (dashed lines corresponding to right y-axis) wind speed. Thermal radiative heat transfer coefficients are approximated as $h_{rg} \approx 4\sigma\epsilon_g T_f^3$ for the black globe and $h_{rw} \approx 4\sigma\epsilon_w T_f^3$ for the wet wick, with $\epsilon_g = \epsilon_w = 0.95$. Surface pressure has a minor impact on all heat transfer coefficients within its typical range of variation, and is fixed at 1000 hPa.

220 via convection and thermal radiation. However, it might be of greater concern for the
 221 evaporative heat transfer coefficient (Eq. 7), as h_{ew} varies by around 2-3% per °C change
 222 in T_{nw} , and evaporation is the most efficient energy loss pathway for the wet wick (Fig.
 223 1b and d).

224 Therefore, a reasonably good first guess for T_{nw} is needed. We choose the wet-bulb
 225 temperature (T_w) which is very close to T_{nw} at night and typically remains within 3°C
 226 below T_{nw} during the day, depending on solar radiation intensity (Fig. 5b). For the sake
 227 of computational efficiency and analytic tractability, we calculate T_w from temperature
 228 and relative humidity using an empirical formula developed by Stull (2011). Stull's T_w
 229 is subject to around 1°C overestimation at high temperatures, commonly occurring dur-
 230 ing the day (Buzan et al., 2015). This slight overestimation actually brings Stull's T_w
 231 closer to T_{nw} and provides a better initial guess. The resulting analytic approximation
 232 is

$$\widehat{T}_{nw} = T_a + \frac{SR_w - \widehat{\beta}(e_{sat}(T_a) - e_a) + LR_w - \sigma\epsilon_w T_a^4}{\widehat{h}_{ew} + \widehat{h}_{cw} + \widehat{h}_{rw}} \quad (11)$$

233 where $\widehat{\beta} = \widehat{k}_x M_{H_2O} \Delta H / P$. By comparing against Eq. 6, we quantify the bias of
 234 \widehat{T}_{nw}

$$\widehat{T}_{nw} - T_{nw} = \eta(T_{nw} - T_a)(T_{nw} - T_w) \quad (12)$$

235

$$\eta = \frac{\frac{1}{2}\beta \frac{\partial^2 e_{sat}(T)}{\partial T^2} \Big|_{T=\frac{T_{nw}+T_w+2T_a}{4}} + \sigma\epsilon_w(T_{nw}^2 + T_w^2 + T_a^2 + T_{nw}T_w + T_aT_{nw} + T_aT_w)}{\widehat{h}_{ew} + \widehat{h}_{cw} + \widehat{h}_{rw}}$$

236 where we assume $\widehat{k}_x \approx k_x$ and $\widehat{h}_{cw} \approx h_{cw}$ since both the convective mass and
 237 heat transfer coefficients are extremely insensitive to variations in film temperature (Fig.
 238 1b-d). Since $T_{nw} \geq T_w$, \widehat{T}_{nw} is subject to overestimation when $T_{nw} > T_a$ and under-
 239 estimation otherwise. By inspection, it is clear that the magnitude of biases increases
 240 with enlarging differences between T_{nw} and both T_a and T_w . Over subtropical hot-dry
 241 regions, the strong VPD cooling and solar radiative heating are expected to enlarge both
 242 temperature gradients with $T_{nw} < T_a$ and $T_{nw} > T_w$ leading to relatively strong neg-
 243 ative biases in \widehat{T}_{nw} .

244 3.3 Wet-bulb globe temperature

245 Substituting \widehat{T}_g (Eq. 9) and \widehat{T}_{nw} (Eq. 11) back into Eq. 1, we obtain the analytic
 246 approximation to WBGT

$$WBGT = 0.7\widehat{T}_{nw} + 0.2\widehat{T}_g + 0.1T_a \quad (13)$$

247 \widehat{T}_g , \widehat{T}_{nw} and $WBGT$ are referred as analytic approximations in the sense that self-
 248 nonlinearities in T_g and T_{nw} within the energy balance equations are eliminated by sub-
 249 stituting initial estimates of them into the mass and/or heat transfer coefficients. This
 250 permits WBGT to be expressed as an analytic function of temperature, humidity, wind
 251 and radiation, although this function remains highly complex and nonlinear.

252 4 Validation of the analytic approximation

253 The validation of the analytic approximation is undertaken in both an idealized
 254 and a more realistic context by comparing against results from Liljegren's full model driven

255 by atmospheric variable inputs. In the idealized setting, we investigate the bias struc-
 256 ture of the analytic approximation across a multidimensional parameter space of air tem-
 257 perature, wind speed, relative humidity and incoming solar radiation based on synthetic
 258 data. We highlight the environmental conditions that yield relatively large biases.

259 Next, we examine the magnitude and spatial distribution of biases within a more
 260 realistic setting using ERA5 reanalysis (Hersbach, H. et al., 2018) for the period 2013-
 261 2022 as the inputs. Since we aim to use this approximate framework in a range of cli-
 262 mate states, including a much warmer future, we also validate it against a "hot" CMIP6
 263 simulation. This is conducted for the period 2091-2100 under the SSP585 scenario us-
 264 ing the ACCESS-CM2 model (Dix et al., 2019) which has a relatively high equilibrium
 265 climate sensitivity of 4.7°C (Hausfather, 2019). The data is evaluated at hourly inter-
 266 vals for ERA5 and 3-hourly for ACCESS-CM2 at their original grid spacing. WBGT is
 267 calculated from 2m air temperature and humidity, 10m wind speed, surface pressure, as
 268 well as surface downward and upwelling flux of long-wave and short-wave radiation.

269 4.1 Validation and bias characterization: idealized setting

270 The accuracy of the analytic approximation is evaluated across a range of air tem-
 271 perature (20-50°C) and wind speed (0.13-3 m/s) under different levels of relative humid-
 272 ity (20% and 60%) and incoming solar radiation (0, 450, and 900 W/m²) (Fig. 2).

273 \widehat{T}_g slightly overestimates T_g in Liljegren's full model by less than 0.2 °C during night-
 274 time and under conditions of moderate solar radiation (450W/m²). However, as solar
 275 radiation intensifies and wind speed diminishes, the degree of overestimation becomes
 276 more pronounced. It can exceed 1 °C under scenarios of strong solar radiation (900 W/m²)
 277 and low wind speed (< 0.5m/s) (Fig. 2a). This intensification of overestimation can be
 278 attributed to the increased temperature gradient between the black globe and the amb-
 279 ient air (as illustrated in Eq. 10) due to intense solar heating and less effective energy
 280 loss through convection under low wind speed. In practice, the relatively large overes-
 281 timation under low wind speed is less a concern as the movement of human body cre-
 282 ates relative air flow especially for outdoor workers. In fact, prior studies frequently as-
 283 sume a minimum wind speed of 1m/s when assessing heat stress-induced labor loss (Casanueva
 284 et al., 2020; Kjellstrom et al., 2018; Bröde et al., 2018).

285 \widehat{T}_{nw} has small biases (within $\pm 0.2^\circ\text{C}$ of T_{nw} in Liljeren's full model) at nighttime
 286 when T_w , our initial estimate, is close to T_{nw} (Fig. 5b). At daytime, \widehat{T}_{nw} performs well
 287 under wet condition (60% relative humidity). However, under dry condition (20% rel-
 288 ative humidity), \widehat{T}_{nw} shows substantial underestimations especially under lower wind speed
 289 and higher temperature where the underestimation can extend up to -2°C. This can be
 290 attributed to a strong temperature gradient between the wet wick and the ambient air
 291 ($T_{nw} - T_a$) under hot-dry conditions with low wind speed (as illustrated in Eq. 12). The
 292 underestimation also intensifies under stronger solar radiation probably owing to an en-
 293 larged difference between T_{nw} and T_w .

294 Biases in \widehat{WBGT} are expected to be primarily influenced by biases in \widehat{T}_{nw} , given
 295 that T_{nw} contributes 70% to WBGT. Accordingly, we found that \widehat{WBGT} shares a simi-
 296 lar bias structure with \widehat{T}_{nw} , but the magnitudes are smaller and within $\pm 0.8^\circ\text{C}$ across
 297 the selected ranges of meteorological conditions (Fig. 2c).

298 4.2 Validation and bias characterization: realistic setting

299 The bias characterization within the idealized setting demonstrates the structure
 300 of biases in the analytic approximations across a range of meteorological conditions. In
 301 practice, those meteorological conditions are not equally sampled with some combina-
 302 tions of temperature, humidity, solar radiation and/or wind speed more or less likely. It

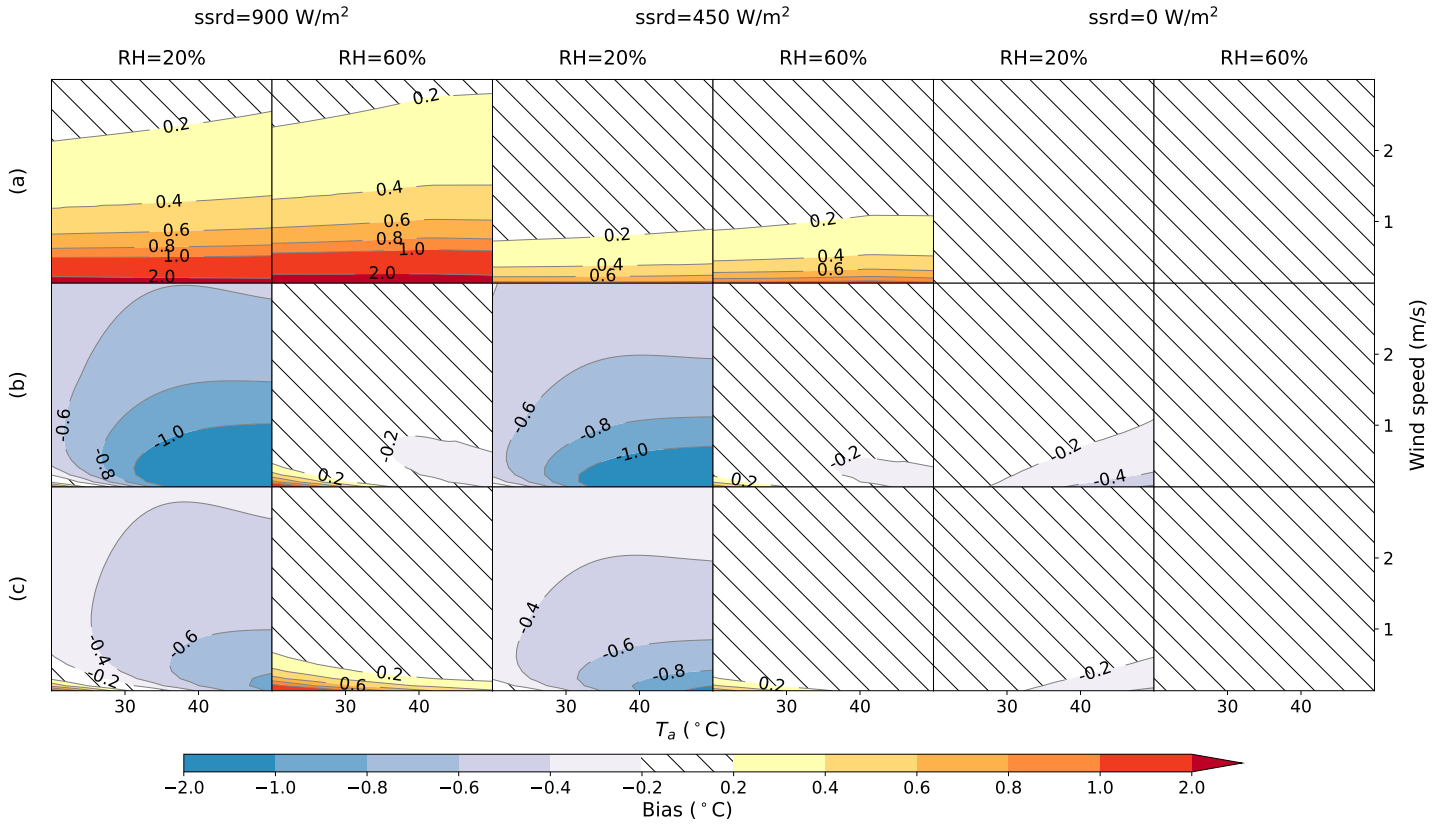


Figure 2. Biases in analytic approximations of (a) T_g , (b) T_{nw} and (c) WBGT across the parameter space covering selected ranges of temperature (T_a) (20-50°C), wind speed (0.13-3m/s), relative humidity (RH) (20%, 60%) and incoming solar radiation (ssrd) (0, 450, 900W/m²). Biases are evaluated against Liljegren’s full model. Thermal radiation and surface reflected solar radiation are approximated from temperature, relative humidity and an assumed surface albedo following the original formulation of Liljegren et al. (2008).

303 is of interest to examine the likely magnitudes and spatial distribution of biases in more
 304 realistic settings.

305 Figure 3 shows the area-weighted empirical distribution of biases in \widehat{WBGT} over
 306 land. During the period 2013-2022 of ERA5, around 78% of the total samples have bi-
 307 ases within $\pm 0.1^\circ\text{C}$, while this percentage extends to 97% for biases within $\pm 0.5^\circ\text{C}$. A
 308 similar level of accuracy is maintained in a warmer world with 93% of samples falling
 309 within $\pm 0.5^\circ\text{C}$. Although the peak of the distribution around zero becomes lower, accom-
 310 panied by a slightly fatter tail on the side of negative biases (Fig. 3), it is unclear whether
 311 this accuracy reduction can be attributed to climate change (Sherwood & Huber, 2010;
 312 Williams et al., 2009), or due to potential effects from other confounding factors such
 313 as the distinct spatial resolutions between ERA5 and ACCESS-CM2. For our purpose
 314 however, the method is sufficiently accurate across a wide range of climates.

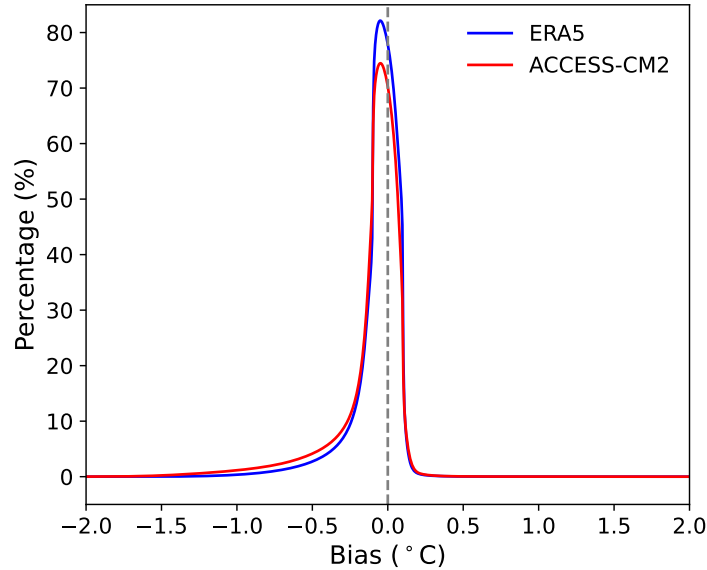


Figure 3. Empirical probability distribution of biases in our analytic approximation \widehat{WBGT} . The y-axes are designed to represent the percentage of samples showing biases within a 0.2°C interval centered on the corresponding x coordinates. The empirical distribution is derived from land data weighted by grid-cell area using ERA5 reanalysis for the period 2013-2022 and the ACCESS-CM2 model for the period 2091-2100 under the SSP585 scenario. Samples with \widehat{WBGT} below 15°C are excluded, as they are less relevant to heat stress.

315 Using ERA5, we then highlight the annual 1% and 99% percentile of these biases,
 316 thereby directing attention to the tails of the bias distribution and their spatial patterns
 317 (Fig. 4). \widehat{T}_g , as demonstrated in Eq. 10, is only subject to overestimations the 1% per-
 318 centile of which is close to zero (Fig. 4a). The 99% percentile of the overestimations is
 319 within 1°C over 97% of global land area (Fig. 4b and k). Over some alpine areas, like
 320 the Himalayas, strong solar radiation stemming from an optically thin atmosphere leads
 321 to large disparities between T_g and T_a , thereby causing relatively strong overestimations
 322 ($>1.8^\circ\text{C}$) (Fig. 4b).

323 In comparison, \widehat{T}_{nw} , can cause both under- and overestimations. The 1% percentile
 324 of biases is characterized by underestimations within -1°C over 85% of land area (Fig.
 325 4d and j). Over subtropical dry regions, strong VPD and solar radiation make T_{nw} sub-
 326 stantially smaller than T_a and larger than T_w which induces more pronounced under-

estimations by \widehat{T}_{nw} (Fig. 4d) as demonstrated in Eq. 12. The 99% percentile of biases show weak overestimations within 0.6°C over 92% of land area (Fig. 4e and k). Over the Himalayas alpine region, small VPD (as a result of cold temperature) and strong solar radiation make T_{nw} considerably larger than both T_a and T_w leading to relatively strong overestimations (Fig. 4e).

\widehat{WBGT} shares a similar spatial distribution of biases as \widehat{T}_{nw} with the 1% percentile of biases showing underestimations within -1°C over 96% of land area (Fig. 4g and j), and the 99% percentile characterized by overestimations within 0.6°C over 94% of land area (Fig. 4h and k).

We also show the 99% percentile of the absolute values of biases in the analytic approximations (Fig. 4 c, f, i and l) in order to highlight the upper tail of the magnitudes of their deviations from Liljegren's full model. In 99% cases, biases in \widehat{T}_g , \widehat{T}_{nw} and \widehat{WBGT} are limited within $\pm 1^{\circ}\text{C}$ over 97%, 82% and 93% of land area. It is also of interest to know the performance of our analytic approximation in representing heat stress at the levels of annual mean and different percentiles. As shown in figure 6q-t, \widehat{WBGT} can well represent heat stress across annual mean and 75%, 90% and 99% percentiles with biases within $\pm 0.5^{\circ}\text{C}$ globally.

4.3 Comparison against other approximations

We compare \widehat{WBGT} against several other WBGT approximations commonly used in the literature. These include sWBGT which only contains temperature and humidity while assuming moderately strong solar radiation and low wind speeds (Australian Bureau of Meteorology, 2010), the environmental stress index (ESI), derived through a multivariate regression of WBGT against temperature, incoming solar radiation, and relative humidity (Moran et al., 2001), the indoor WBGT ($WBGT_{in}$) which substitutes T_{nw} with the thermodynamic wet-bulb temperature (T_w) and T_g with T_a (Dunne et al., 2013; C. Li et al., 2020; D. Li et al., 2020), and the one recently developed by Brimicombe et al. (2023) ($WBGT_{Br}$) which calculates T_g from mean radiant temperature, and approximates T_{nw} using Stull's T_w formulation (Stull, 2011).

Figure 5a illustrates the empirical bias distribution of these approximations along with that of our analytic approximation based on ERA5. \widehat{WBGT} clearly outperforms others. sWBGT performs the worst, and its bias distribution peaks at an overestimation of approximately 5°C due to the implicit assumption of moderately strong solar radiation. This overestimate can profoundly affect future heat stress projections and estimate of impact on people (de Lima et al., 2021). Therefore, we do not recommend the continued use of sWBGT. ESI performs significantly better with a relatively symmetric distribution of biases centered around zero.

The distribution of biases in both $WBGT_{in}$ and $WBGT_{Br}$ have a primary peak near zero as well as secondary peaks corresponding to underestimations of approximately -2.4°C and -1.2°C respectively (Fig. 5a). Both $WBGT_{in}$ and $WBGT_{Br}$ substitute T_{nw} with T_w , and $WBGT_{in}$ also approximates T_g with T_a . These approximations work relatively well during nighttime especially for T_{nw} (Fig. 5b). Notably, T_g is lower than T_a at nighttime, and the distribution of their differences peaks around -1°C , but can extend up to -3°C (Fig. 5b). That is because air is not a black body, and consequently the long-wave radiative exchange between the black globe and ambient air produce net cooling on the globe. However, during daytime, T_w and T_a significantly underestimate T_{nw} and T_g due to the omission of solar radiative heating. The distributions of these underestimations peak around -1.2°C and -7.6°C respectively (Fig. 5b) which amounts to underestimations in WBGT of -0.8°C and -1.5°C given the weights on T_{nw} and T_g in WBGT formulation. The differentiated daytime versus nighttime performances explain the bimodal distribution of biases in $WBGT_{in}$ and $WBGT_{Br}$ (Fig. 5a).

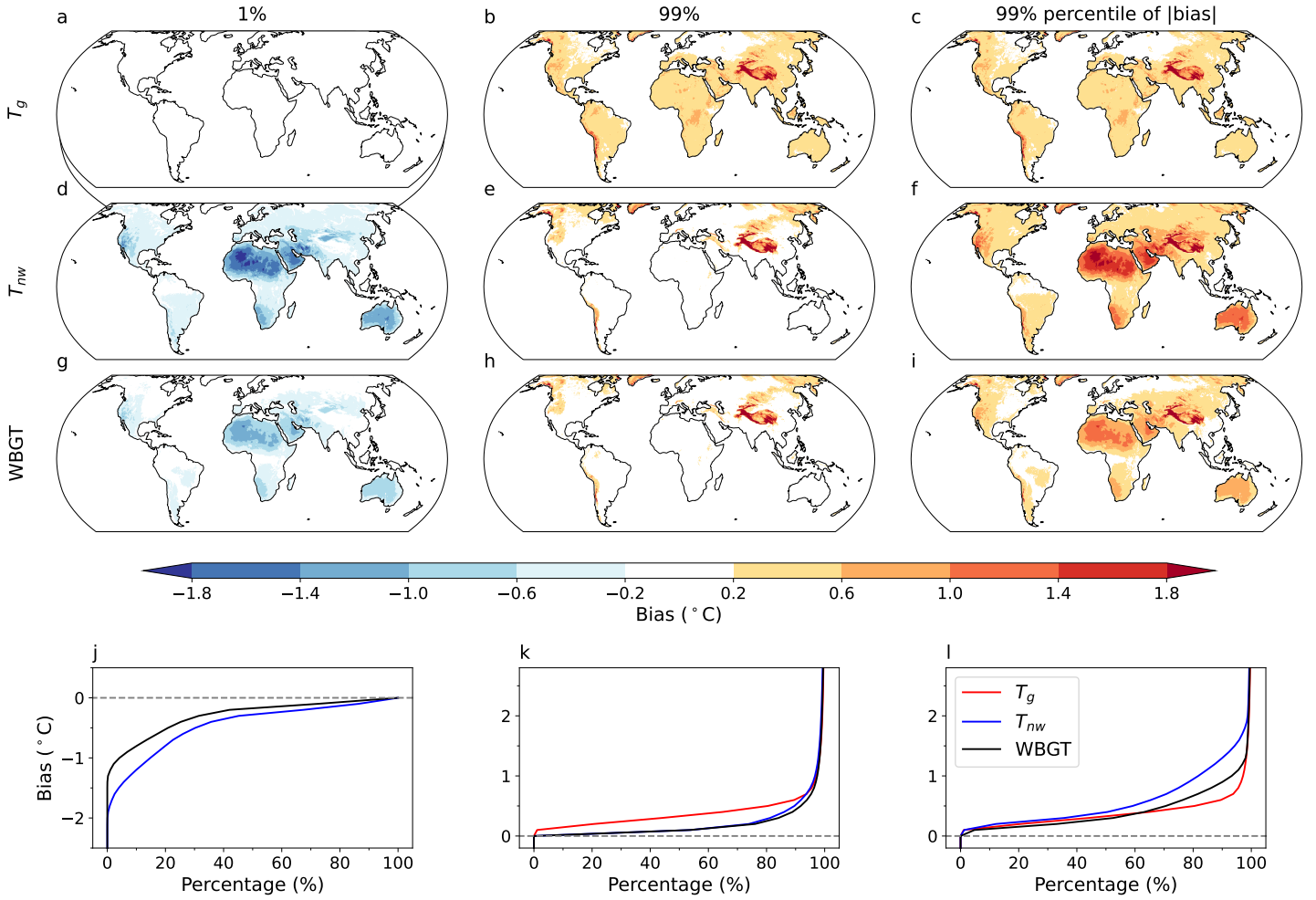


Figure 4. Annual (left) 1% and (middle) 99% percentile of biases, and (right) 99% percentile of the absolute magnitudes of biases in the analytic approximations of (a-c) T_g , (d-f) T_{nw} and (g-i) WBGT. Panels j-l represent the empirical cumulative distribution of these biases across all continental grid cells weighted by area. The 1% percentile of biases in \hat{T}_g are very close to zero and therefore are omitted in (j). Biases are evaluated by comparing against Liljegren's full model based on hourly ERA5 reanalysis data during 2013-2022.

377 The shape of the bias distribution and the relative performance of different approx-
 378 imations remain consistent in a future warmer world, where \widehat{WBGT} continues to have
 379 the best performance (Fig. 5c).

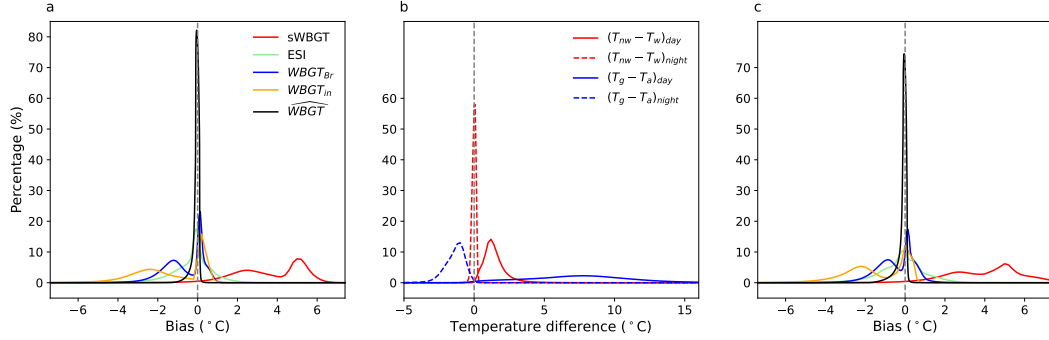


Figure 5. Empirical probability distribution of (a) biases in our analytic formulation \widehat{WBGT} and several other WBGT approximations, and (b) $T_{nw} - T_w$ and $T_g - T_a$ at both daytime and nighttime. Both (a) and (b) are derived from land data weighted by grid-cell area using ERA5 reanalysis for the period of 2013-2022. Panel (c) is the same as (a) except for the period 2091-2100 under the SSP585 scenario using the ACCESS-CM2 model. The y-axes are designed to represent the percentage of samples showing biases within a 0.2 °C interval centered on the corresponding x coordinates. Samples with WBGT below 15°C are excluded, as they are less relevant to heat stress.

380 Our analytic approximation also performs better in representing the annual mean
 381 and 75-99% percentiles of WBGT with biases consistently within $\pm 0.5^\circ\text{C}$ across the world
 382 as described previously (Fig. 6). sWBGT strongly overestimates WBGT especially at
 383 annual mean level, and this overestimation becomes weaker towards higher percentiles
 384 where the assumption of moderately strong solar radiation becomes more applicable (Fig.
 385 6a-d). ESI performs well in capturing annual mean and 75% percentile of WBGT with
 386 biases mostly within $\pm 1^\circ\text{C}$, but considerably underestimates the 99% percentile by up
 387 to -4°C across the low latitudes (Fig. 6e-h). Both $WBGT_{in}$ and $WBGT_{Br}$ consistently
 388 show underestimations the magnitude of which increases towards higher percentiles (Fig.
 389 6i-p). Among them, $WBGT_{Br}$ has better performance since T_g is calculated from mean
 390 radiant temperature rather than replaced with T_a as is done for $WBGT_{in}$.

391 5 Summary and implication

392 We have developed an approximate form of WBGT that does not require iterative
 393 calculation. The need for iteration in WBGT calculation arises from the nonlinear de-
 394 pendence of mass and/or heat transfer (through convection, thermal radiation and evap-
 395 oration) efficiencies on T_g or T_{nw} , rendering the energy balance equations analytically
 396 intractable. However, we have shown that this dependence is weak for convection which
 397 is primarily influenced by wind speed. This self-dependence is also of minor importance
 398 for thermal radiation because the thermal radiative heat transfer coefficient changes by
 399 a small fraction within the typical variation range of T_g or T_{nw} , and energy loss via ther-
 400 mal radiation is much less efficient than convection and evaporation. The dependence
 401 of evaporative heat transfer coefficient on T_{nw} is of greater concern since h_{ew} is relatively
 402 sensitive to T_{nw} variations (h_{ew} varies by 2-3% per °C change in T_{nw}) and evaporation
 403 plays a dominant role in the energy loss of the wet wick.

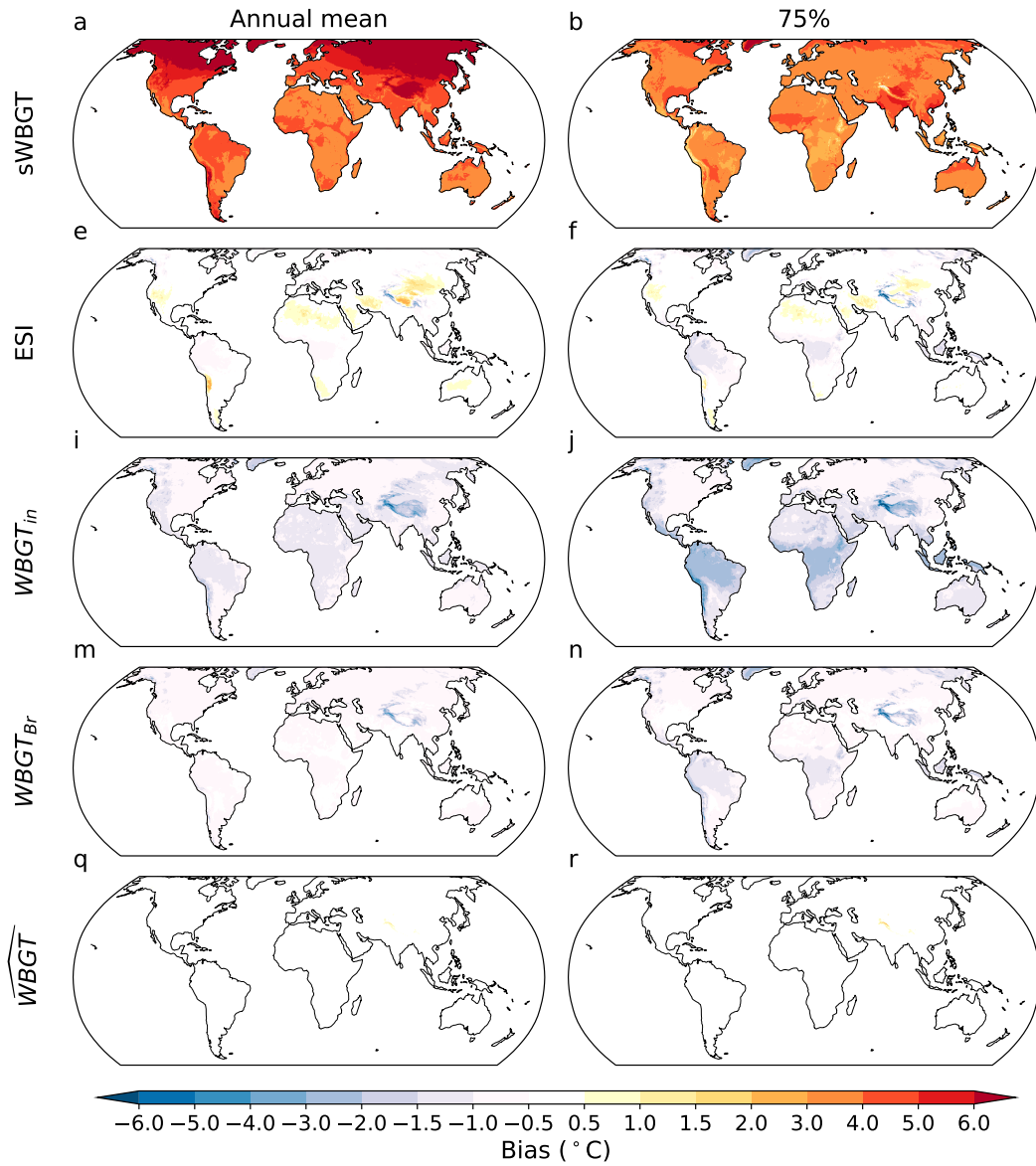


Figure 6. Biases in the annual mean and 75%, 90% and 99% percentile values of our analytic approximation (\widehat{WBGT}) and several other approximations of WBGT. Biases are evaluated by comparing against Liljegren's full model based on hourly ERA5 reanalysis data during 2013-2022.

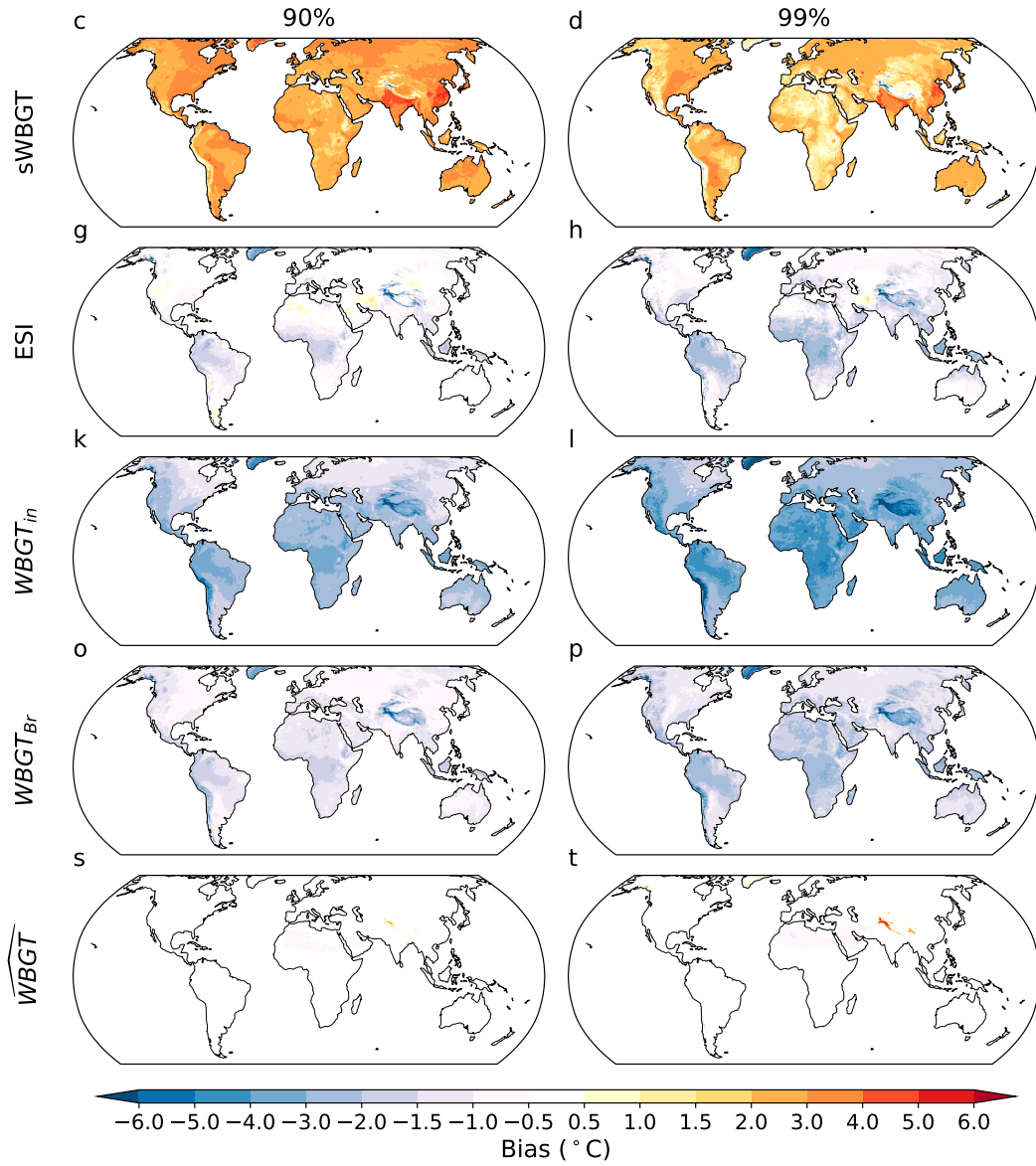


Figure 6. Continued.

404 The recognition of the weak self-nonlinearity, at least for convection and thermal
 405 radiation, motivates the development of an analytic approximation of WBGT by sub-
 406 stituting T_a and T_w as initial estimates for T_g and T_{nw} into the mass and heat transfer
 407 coefficients. The analytic approximation eliminates the need for iteration and is more
 408 accurate than other WBGT approximations commonly used in the literature. It presents
 409 an useful first guess to Liljegren's full model given its reasonably high accuracy and com-
 410 putational straightforwardness. However, users should consider the potential underes-
 411 timation of heat stress under extremely hot-dry conditions. Notably, more accurate es-
 412 timates can be obtained through a single iteration, with the analytic approximations serv-
 413 ing as the updated first guesses. Recently, Liljeren's WBGT formulation has been im-
 414 plemented into the Community Land Model Version 5 (CLM5) for non-urban settings
 415 (Buzan, 2024). Our analytic approximation could offer an useful alternative for inclu-
 416 sion in the model to prevent the model from slowing down due to iterative WBGT cal-
 417 culations.

418 The complex, nonlinear interactions between multiple meteorological parameters
 419 not only require WBGT to be calculated iteratively, but also lead to a functional form
 420 that is opaque to theoretical investigation and often times treated as a black box. As a
 421 result, WBGT—despite being a good representation of human heat stress—has not been
 422 adopted for understanding the atmospheric dynamics and thermodynamic processes contr-
 423 trolling heat stress. Instead, strictly thermodynamic variables like T_w , moist enthalpy
 424 or equivalent potential temperature are used for such purpose because of their straight-
 425 forward dynamic and thermodynamic constraint (Kong & Huber, 2023; Raymond et al.,
 426 2021; Zhang et al., 2021; Lutsko, 2021). But these thermodynamic quantities are not in-
 427 tended for or well calibrated to human heat stress which diminishes the practical rele-
 428 vance of the generated insights (Simpson et al., 2023; Lu & Romps, 2023).

429 In deriving the analytic approximation, we have gained insights that the deviation
 430 of both T_g and T_{nw} from T_a is controlled by the ratio between solar radiative heating
 431 (and VPD cooling for T_{nw}) and the efficiency of energy loss through convection and long-
 432 wave cooling (and evaporation for T_{nw}) (Eq. 4 and 8). Therefore, understanding changes
 433 in T_g , T_{nw} and consequently WBGT, must involve strong constraints or knowledge of
 434 the evolution of this ratio. Depending on the problem under consideration, if solar ra-
 435 diation and wind speed remain unchanged, the ratio for T_g (Eq. 4) is approximately con-
 436 stant given minor influence from changes in thermal radiative heat transfer efficiency.
 437 Consequently, T_g is expected to vary at the same rate as T_a . It is less straightforward
 438 to get a quick, simple relation between changes in T_{nw} and T_a , as the ratio in Eq. 8 also
 439 depends on humidity and T_{nw} itself due to the VPD cooling term and evaporative heat
 440 transfer coefficient. Nevertheless, given certain assumptions on humidity changes (e.g.,
 441 constant relative humidity), we should be able to explicitly predict how T_{nw} scales with
 442 temperature as well. In addition, since T_{nw} is driven away from T_w by solar radiation
 443 under the modulation of wind, we may expect the differences between them to be roughly
 444 constant if both solar radiation and wind remain unchanged. If this is the case, the scal-
 445 ing of T_{nw} and T_w with temperature should be close to each other.

446 More generally, Eq. 4 and Eq. 8, with their clear physical interpretation, may serve
 447 as a starting point for an analytic investigation of the sensitivity of WBGT to changes
 448 in temperature, humidity, wind and solar radiation. Clearly, we have better intuition on
 449 these traditional meteorological parameters, and established theories to constrain their
 450 variations (Zhang & Boos, 2023; Byrne, 2021; Byrne & O'Gorman, 2013, 2016; McColl
 451 & Tang, 2024). An explicit, analytic expression of WBGT's sensitivity to these tradi-
 452 tional meteorological variables helps remove the obscuring veil of WBGT's apparent com-
 453 plexity and may facilitate its application in understanding the physical control of heat
 454 stress. For example, we can quantitatively disentangle the relative role of changes in each
 455 meteorological input and the underlying physical processes in explaining WBGT responses

456 to any physical perturbations (like atmospheric blocking events, irrigation or increasing
457 greenhouse gas emission). These will be further explored in upcoming studies.

458 6 Open Research

459 Hersbach, H. et al. (2018) was downloaded from the Copernicus Climate Change
460 Service (C3S) Climate Data Store (<https://cds.climate.copernicus.eu/cdsapp#!/dataset/reanalysis-era5-single-levels?tab=form>). The results contain modified
461 Copernicus Climate Change Service information 2020. Neither the European Commis-
462 sion nor ECMWF is responsible for any use that may be made of the Copernicus infor-
463 mation or data it contains. Dix et al. (2019) was downloaded from [https://esgf-index1
464 .ceda.ac.uk/search/cmip6-ceda/](https://esgf-index1.ceda.ac.uk/search/cmip6-ceda/). Liljegren's WBGT code in C language is accessi-
465 ble at <https://github.com/mdljts/wbgt/blob/master/src/wbgt.c>, and was ported
466 to Cython (can be compiled and implemented in Python) by Kong and Huber (2022)
467 (available at <https://zenodo.org/record/5980536>). The code for the analytic WBGT
468 approximation is deposited at Zenodo (<https://zenodo.org/records/10802580>) along
469 with a Jupyter notebook to introduce its usage. The following Python packages were utilised:
470 Numpy (Harris et al., 2020), Xarray (Hoyer & Hamman, 2017), Dask (Dask Develop-
471 ment Team, 2016), Matplotlib (Hunter, 2007), and Cartopy (Met Office, 2010 - 2015).
472

473 Acknowledgments

474 This study is Funded by NASA FINESST grant 80NSSC22K1544, grant NSF 1805808-
475 CBET Innovations at the Nexus of Food, Energy, and Water Systems (INFEWS: U.S.-
476 China): A multi-scale integrated modeling approach to managing the transition to sus-
477 tainability and NSF 1829764-OAC CyberTraining: CIU:Cross-disciplinary Training for
478 Findable, Accessible, Interoperable, and Reusable (FAIR) science. We thank Rodrigo
479 Caballero for useful discussions that clarified the presentation of concepts in this study.
480 The authors declare no competing interests.

481 References

- 482 ACSM. (1984). *Position stand on the prevention of thermal injuries during distance*
483 *running* (Tech. Rep.). Medicine Sci. Sport. Exercise.
- 484 Army, U. (2003). *Heat stress control and heat casualty management* (Tech. Rep.).
485 Technical Bulletin Medical 507/Air Force Pamphlet.
- 486 Australian Bureau of Meteorology. (2010). *About the approximation to the*
487 *WBGT used by the Bureau of Meteorology*. Retrieved 2021-04-03, from
488 http://www.bom.gov.au/info/thermal_stress/#approximation
- 489 Bedingfield, C. H., & Drew, T. B. (1950). Analogy between Heat Transfer and Mass
490 Transfer. *Industrial & Engineering Chemistry*, 42(6), 1164–1173. doi: 10.1021/
491 ie50486a029
- 492 Brenda Jacklitsch, W. Jon Williams, Kristin Musolin, Aitor Coca, Jung-Hyun Kim,
493 & Nina Turner. (2016). *Criteria for a Recommended Standard: Occupational*
494 *Exposure to Heat and Hot Environments* (Tech. Rep. No. DHHS (NIOSH)
495 Publication No. 2016-106). Washington, D.C: DHHS, NIOSH.
- 496 Brimicombe, C., Lo, C. H. B., Pappenberger, F., Di Napoli, C., Maciel, P., Quintino,
497 T., . . . Cloke, H. L. (2023). Wet Bulb Globe Temperature: Indicating Extreme
498 Heat Risk on a Global Grid. *GeoHealth*, 7(2). doi: 10.1029/2022GH000701
- 499 Bröde, P., Fiala, D., Lemke, B., & Kjellstrom, T. (2018). Estimated work abil-
500 ity in warm outdoor environments depends on the chosen heat stress assess-
501 ment metric. *International Journal of Biometeorology*, 62(3), 331–345. doi:
502 10.1007/s00484-017-1346-9
- 503 Burke, M., González, F., Baylis, P., Heft-Neal, S., Baysan, C., Basu, S., &
504 Hsiang, S. (2018). Higher temperatures increase suicide rates in the

- 505 United States and Mexico. *Nature Climate Change*, 8(8), 723–729. doi:
506 10.1038/s41558-018-0222-x
- 507 Burke, M., Hsiang, S. M., & Miguel, E. (2015). Global non-linear effect of temper-
508 ature on economic production. *Nature*, 527(7577), 235–239. doi: 10.1038/
509 nature15725
- 510 Buzan, J. R. (2024). Implementation and Evaluation of Wet Bulb Globe Tempera-
511 ture Within Non-Urban Environments in the Community Land Model Version
512 5. *Journal of Advances in Modeling Earth Systems*, 16(2), e2023MS003704.
513 doi: 10.1029/2023MS003704
- 514 Buzan, J. R., & Huber, M. (2020). Moist Heat Stress on a Hotter Earth. *Annual*
515 *Review of Earth and Planetary Sciences*, 48(1), 623–655. doi: 10.1146/annurev
516 -earth-053018-060100
- 517 Buzan, J. R., Oleson, K., & Huber, M. (2015). Implementation and compari-
518 son of a suite of heat stress metrics within the Community Land Model
519 version 4.5. *Geoscientific Model Development*, 8(2), 151–170. doi:
520 10.5194/gmd-8-151-2015
- 521 Byrne, M. P. (2021). Amplified warming of extreme temperatures over tropical land.
522 *Nature Geoscience*, 14(11), 837–841. doi: 10.1038/s41561-021-00828-8
- 523 Byrne, M. P., & O’Gorman, P. A. (2013). Land–Ocean Warming Contrast
524 over a Wide Range of Climates: Convective Quasi-Equilibrium Theory
525 and Idealized Simulations. *Journal of Climate*, 26(12), 4000–4016. doi:
526 10.1175/JCLI-D-12-00262.1
- 527 Byrne, M. P., & O’Gorman, P. A. (2016). Understanding Decreases in Land Relative
528 Humidity with Global Warming: Conceptual Model and GCM Simulations.
529 *Journal of Climate*, 29(24), 9045–9061. doi: 10.1175/JCLI-D-16-0351.1
- 530 Casanueva, A., Kotlarski, S., Fischer, A. M., Flouris, A. D., Kjellstrom, T., Lemke,
531 B., ... Liniger, M. A. (2020). Escalating environmental summer heat expo-
532 sure—a future threat for the European workforce. *Regional Environmental*
533 *Change*, 20(2), 40. doi: 10.1007/s10113-020-01625-6
- 534 Chavaillaz, Y., Roy, P., Partanen, A.-I., Da Silva, L., Bresson, E., Mengis, N., ...
535 Matthews, H. D. (2019). Exposure to excessive heat and impacts on labour
536 productivity linked to cumulative CO2 emissions. *Scientific Reports*, 9(1),
537 13711. doi: 10.1038/s41598-019-50047-w
- 538 Chilton, T. H., & Colburn, A. P. (1934). Mass Transfer (Absorption) Coefficients
539 Prediction from Data on Heat Transfer and Fluid Friction. *Industrial & Engi-
540 neering Chemistry*, 26(11), 1183–1187. doi: 10.1021/ie50299a012
- 541 Clark, J., & Konrad, C. E. (2023). Observations and Estimates of Wet Bulb Globe
542 Temperature in Varied Microclimates. *Journal of Applied Meteorology and Cli-
543 matology*. doi: 10.1175/JAMC-D-23-0078.1
- 544 Dask Development Team. (2016). Dask: Library for dynamic task scheduling [Com-
545 puter software manual]. Retrieved from <https://dask.org>
- 546 de Freitas, C. R., & Grigorieva, E. A. (2015). A comprehensive catalogue and clas-
547 sification of human thermal climate indices. *International Journal of Biometeo-
548 rology*, 59(1), 109–120. doi: 10.1007/s00484-014-0819-3
- 549 de Lima, C. Z., Buzan, J. R., Moore, F. C., Baldos, U. L. C., Huber, M., & Hertel,
550 T. W. (2021). Heat stress on agricultural workers exacerbates crop impacts
551 of climate change. *Environmental Research Letters*, 16(4), 044020. doi:
552 10.1088/1748-9326/abeb9f
- 553 Dix, M., Bi, D., Dobrohotoff, P., Fiedler, R., Harman, I., Law, R., ... Yang, R.
554 (2019). *CSIRO-ARCCSS ACCESS-CM2 model output prepared for CMIP6*
555 *ScenarioMIP ssp585*. Earth System Grid Federation. Retrieved 2024-02-10,
556 from <http://cera-www.dkrz.de/WDCC/meta/CMIP6/CMIP6.ScenarioMIP>
557 .CSIRO-ARCCSS.ACCESS-CM2.ssp585 (Medium: application/x-netcdf Version
558 Number: 20230220 Type: dataset) doi: 10.22033/ESGF/CMIP6.4332
- 559 Dunne, J. P., Stouffer, R. J., & John, J. G. (2013). Reductions in labour capacity

- 560 from heat stress under climate warming. *Nature Climate Change*, 3(6), 563–
561 566. doi: 10.1038/nclimate1827
- 562 Ebi, K. L., Capon, A., Berry, P., Broderick, C., De Dear, R., Havenith, G., ...
563 Jay, O. (2021). Hot weather and heat extremes: health risks. *The Lancet*,
564 398(10301), 698–708. doi: 10.1016/S0140-6736(21)01208-3
- 565 Foster, J., Smallcombe, J. W., Hodder, S., Jay, O., Flouris, A. D., & Havenith, G.
566 (2022). Quantifying the impact of heat on human physical work capacity; part
567 II: the observed interaction of air velocity with temperature, humidity, sweat
568 rate, and clothing is not captured by most heat stress indices. *International*
569 *Journal of Biometeorology*, 66(3), 507–520. doi: 10.1007/s00484-021-02212-y
- 570 Foster, J., Smallcombe, J. W., Hodder, S., Jay, O., Flouris, A. D., Nybo, L., &
571 Havenith, G. (2022). Quantifying the impact of heat on human physical work
572 capacity; part III: the impact of solar radiation varies with air temperature,
573 humidity, and clothing coverage. *International Journal of Biometeorology*,
574 66(1), 175–188. doi: 10.1007/s00484-021-02205-x
- 575 Gao, J., Wang, Y., Wu, X., Gu, X., & Song, X. (2019). A simplified indoor wet-bulb
576 globe temperature formula to determine acceptable hot environmental paramet-
577 ers in naturally ventilated buildings. *Energy and Buildings*, 196, 169–177. doi:
578 10.1016/j.enbuild.2019.05.035
- 579 Harris, C. R., Millman, K. J., van der Walt, S. J., Gommers, R., Virtanen, P., Cour-
580 napeau, D., ... Oliphant, T. E. (2020). Array programming with NumPy.
581 *Nature*, 585(7825), 357–362. doi: 10.1038/s41586-020-2649-2
- 582 Hausfather, Z. (2019). *Cmip6: The next generation of climate models ex-*
583 *plained*. Retrieved 2024-02-13, from [https://www.carbonbrief.org/
584 cmip6-the-next-generation-of-climate-models-explained](https://www.carbonbrief.org/cmip6-the-next-generation-of-climate-models-explained)
- 585 Havenith, G., & Fiala, D. (2015, December). Thermal Indices and Thermophysiol-
586 ical Modeling for Heat Stress. In R. Terjung (Ed.), *Comprehensive Physiology*
587 (pp. 255–302). Hoboken, NJ, USA: John Wiley & Sons, Inc. Retrieved 2020-
588 06-27, from <http://doi.wiley.com/10.1002/cphy.c140051> doi: 10.1002/
589 cphy.c140051
- 590 Hersbach, H., Bell, B., Berrisford, P., Biavati, G., Horányi, A., Muñoz Sabater, J.,
591 ... Thépaut, J.-N. (2018). ERA5 hourly data on single levels from 1979 to
592 present. *Copernicus Climate Change Service (C3S) Climate Data Store (CDS)*.
593 doi: 10.24381/cds.adbb2d47
- 594 Hoyer, S., & Hamman, J. (2017). xarray: N-D labeled arrays and datasets in
595 Python. *Journal of Open Research Software*, 5(1). doi: 10.5334/jors.148
- 596 Hsiang, S. M., Burke, M., & Miguel, E. (2013). Quantifying the Influence of Cli-
597 mate on Human Conflict. *Science*, 341(6151), 1235367. doi: 10.1126/science
598 .1235367
- 599 Hunter, J. D. (2007). Matplotlib: A 2d graphics environment. *Computing in Science*
600 *& Engineering*, 9(3), 90–95. doi: 10.1109/MCSE.2007.55
- 601 Ioannou, L. G., Tsoutsoubi, L., Mantzios, K., Vliora, M., Nintou, E., Piil, J. F., ...
602 Flouris, A. D. (2022). Indicators to assess physiological heat strain – Part 3:
603 Multi-country field evaluation and consensus recommendations. *Temperature*,
604 9(3), 274–291. doi: 10.1080/23328940.2022.2044739
- 605 ISO. (1998). *Ergonomics of the thermal environment - instruments for measuring*
606 *physical quantities* (International Standard). Geneva: International Organiza-
607 tion for Standardization (ISO).
- 608 ISO. (2017). *Ergonomics of the thermal environment — Assessment of heat stress*
609 *using the WBGT (wet bulb globe temperature) index* (International Standard).
610 Geneva: International Organization for Standardization (ISO).
- 611 Kamal, A. S. M. M., Faruki Fahim, A. K., & Shahid, S. (2024). Simplified equations
612 for wet bulb globe temperature estimation in Bangladesh. *International Jour-*
613 *nal of Climatology*, joc.8402. doi: 10.1002/joc.8402
- 614 Kjellstrom, T., Briggs, D., Freyberg, C., Lemke, B., Otto, M., & Hyatt, O. (2016).

- 615 Heat, Human Performance, and Occupational Health: A Key Issue for the As-
 616 sessment of Global Climate Change Impacts. *Annual Review of Public Health*,
 617 37(1), 97–112. doi: 10.1146/annurev-publhealth-032315-021740
- 618 Kjellstrom, T., Freyberg, C., Lemke, B., Otto, M., & Briggs, D. (2018). Estimating
 619 population heat exposure and impacts on working people in conjunction with
 620 climate change. *International Journal of Biometeorology*, 62(3), 291–306. doi:
 621 10.1007/s00484-017-1407-0
- 622 Kong, Q., & Huber, M. (2022). Explicit calculations of Wet Bulb Globe Tempera-
 623 ture compared with approximations and why it matters for labor productivity.
 624 *Earth's Future*. doi: 10.1029/2021EF002334
- 625 Kong, Q., & Huber, M. (2023). Regimes of soil moisture-wet bulb temperature cou-
 626 pling with relevance to moist heat stress. *Journal of Climate*, 1–45. doi: 10
 627 .1175/JCLI-D-23-0132.1
- 628 Lemke, B., & Kjellstrom, T. (2012). Calculating workplace WBGT from meteorolog-
 629 ical data: a tool for climate change assessment. *Industrial Health*, 50(4), 267–
 630 278. doi: 10.2486/indhealth.MS1352
- 631 Li, C., Sun, Y., Zwiers, F., Wang, D., Zhang, X., Chen, G., & Wu, H. (2020).
 632 Rapid Warming in Summer Wet Bulb Globe Temperature in China with
 633 Human-Induced Climate Change. *Journal of Climate*, 33(13), 5697–5711. doi:
 634 10.1175/JCLI-D-19-0492.1
- 635 Li, D., Yuan, J., & Kopp, R. E. (2020). Escalating global exposure to compound
 636 heat-humidity extremes with warming. *Environmental Research Letters*, 15(6),
 637 064003. doi: 10.1088/1748-9326/ab7d04
- 638 Liljegren, J. C., Carhart, R. A., Lawday, P., Tschopp, S., & Sharp, R. (2008).
 639 Modeling the Wet Bulb Globe Temperature Using Standard Meteorological
 640 Measurements. *Journal of Occupational and Environmental Hygiene*, 5(10),
 641 645–655. doi: 10.1080/15459620802310770
- 642 Lu, Y.-C., & Romps, D. (2023). Wet-Bulb Temperature or Heat Index: Which Bet-
 643 ter Predicts Fatal Heat in a Warming Climate? *Physiology*, 38(S1), 5734524.
 644 doi: 10.1152/physiol.2023.38.S1.5734524
- 645 Lutsko, N. J. (2021). The Relative Contributions of Temperature and Moisture to
 646 Heat Stress Changes under Warming. *Journal of Climate*, 34(3), 901–917. doi:
 647 10.1175/JCLI-D-20-0262.1
- 648 Matsumoto, K., Tachiiri, K., & Su, X. (2021). Heat stress, labor productivity, and
 649 economic impacts: analysis of climate change impacts using two-way coupled
 650 modeling. *Environmental Research Communications*, 3(12), 125001. doi:
 651 10.1088/2515-7620/ac3e14
- 652 McColl, K. A., & Tang, L. I. (2024). An Analytic Theory of Near-Surface Relative
 653 Humidity over Land. *Journal of Climate*, 37(4), 1213–1230. doi: 10.1175/JCLI
 654 -D-23-0342.1
- 655 Met Office. (2010 - 2015). Cartopy: a cartographic python library with a mat-
 656 plotlib interface [Computer software manual]. Exeter, Devon. Retrieved from
 657 <https://scitools.org.uk/cartopy>
- 658 Moran, D., Pandolf, K., Shapiro, Y., Heled, Y., Shani, Y., Mathew, W., & Gonza-
 659 lez, R. (2001). An environmental stress index (ESI) as a substitute for the
 660 wet bulb globe temperature (WBGT). *Journal of Thermal Biology*, 26(4-5),
 661 427–431. doi: 10.1016/S0306-4565(01)00055-9
- 662 NIOSH. (2016). *Criteria for a Recommended Standard: Occupational Exposure to*
 663 *Heat and Hot Environments* (Tech. Rep. No. DHHS (NIOSH) Publication No.
 664 2016-106). Washington, D.C: DHHS, NIOSH.
- 665 Orlov, A., De Hertog, S., Havermann, F., Guo, S., Luo, F., Manola, I., . . . Schleuss-
 666 ner, C. (2023). Changes in Land Cover and Management Affect Heat
 667 Stress and Labor Capacity. *Earth's Future*, 11(3), e2022EF002909. doi:
 668 10.1029/2022EF002909
- 669 OSHA. (2017). *Osha technical manual, section iii, chapter 4:heat stress*. (Tech. Rep.

- 670 No. TED-01-00-015). Washington (DC): U.S. Department of Labor, OSHA:
 671 Occupational Safety and Health Administration (OSHA).
- 672 Patel, T., Mullen, S. P., & Santee, W. R. (2013). Comparison of Methods
 673 for Estimating Wet-Bulb Globe Temperature Index From Standard Me-
 674 teorological Measurements. *Military Medicine*, *178*(8), 926–933. doi:
 675 10.7205/MILMED-D-13-00117
- 676 Raymond, C., Matthews, T., Horton, R. M., Fischer, E. M., Fueglistaler, S.,
 677 Ivanovich, C., ... Zhang, Y. (2021). On the Controlling Factors for Glob-
 678 ally Extreme Humid Heat. *Geophysical Research Letters*, *48*(23). doi:
 679 10.1029/2021GL096082
- 680 Saeed, W., Haqiqi, I., Kong, Q., Huber, M., Buzan, J. R., Chonabayashi, S.,
 681 ... Hertel, T. W. (2022). The Poverty Impacts of Labor Heat Stress
 682 in West Africa Under a Warming Climate. *Earth's Future*, *10*(11). doi:
 683 10.1029/2022EF002777
- 684 Sherwood, S. C., & Huber, M. (2010). An adaptability limit to climate change
 685 due to heat stress. *Proceedings of the National Academy of Sciences*, *107*(21),
 686 9552–9555. doi: 10.1073/pnas.0913352107
- 687 Simpson, C. H., Brousse, O., Ebi, K. L., & Heaviside, C. (2023). Commonly used in-
 688 dices disagree about the effect of moisture on heat stress. *npj Climate and At-
 689 mospheric Science*, *6*(1), 78. doi: 10.1038/s41612-023-00408-0
- 690 Stull, R. (2011). Wet-Bulb Temperature from Relative Humidity and Air Tempera-
 691 ture. *Journal of Applied Meteorology and Climatology*, *50*(11), 2267–2269. doi:
 692 10.1175/JAMC-D-11-0143.1
- 693 Tuholske, C., Caylor, K., Funk, C., Verdin, A., Sweeney, S., Grace, K., ... Evans,
 694 T. (2021, October). Global urban population exposure to extreme heat. *Pro-
 695 ceedings of the National Academy of Sciences*, *118*(41), e2024792118. doi:
 696 10.1073/pnas.2024792118
- 697 Vecellio, D. J., Wolf, S. T., Cottle, R. M., & Kenney, W. L. (2022). Utility of the
 698 Heat Index in defining the upper limits of thermal balance during light phys-
 699 ical activity (PSU HEAT Project). *International Journal of Biometeorology*,
 700 *66*(9), 1759–1769. doi: 10.1007/s00484-022-02316-z
- 701 Williams, I. N., Pierrehumbert, R. T., & Huber, M. (2009). Global warming, con-
 702 vective threshold and false thermostats. *Geophysical Research Letters*, *36*(21),
 703 L21805. doi: 10.1029/2009GL039849
- 704 Yaglou, C. P., & Minard, D. (1957). Control of heat casualties at military training
 705 centers. *A.M.A. archives of industrial health*, *16*(4), 302–316.
- 706 Zhang, Y., & Boos, W. R. (2023). An upper bound for extreme temperatures over
 707 midlatitude land. *Proceedings of the National Academy of Sciences*, *120*(12),
 708 e2215278120. doi: 10.1073/pnas.2215278120
- 709 Zhang, Y., Held, I., & Fueglistaler, S. (2021). Projections of tropical heat stress con-
 710 strained by atmospheric dynamics. *Nature Geoscience*, *14*(3), 133–137. doi: 10
 711 .1038/s41561-021-00695-3
- 712 Zhang, Y., & Shindell, D. T. (2021). Costs from labor losses due to extreme heat in
 713 the USA attributable to climate change. *Climatic Change*, *164*(3-4), 35. doi:
 714 10.1007/s10584-021-03014-2
- 715 Zhu, J., Wang, S., Zhang, B., & Wang, D. (2021). Adapting to Changing Labor Pro-
 716 ductivity as a Result of Intensified Heat Stress in a Changing Climate. *Geo-
 717 Health*, *5*(4). doi: 10.1029/2020GH000313